

Sediment flux driven channel geometry adjustment of bedrock and mixed gravel-bedrock rivers

Edwin Baynes, Dimitri Lague, Philippe Steer, Stéphane Bonnet, Luc Illien

▶ **To cite this version:**

Edwin Baynes, Dimitri Lague, Philippe Steer, Stéphane Bonnet, Luc Illien. Sediment flux driven channel geometry adjustment of bedrock and mixed gravel-bedrock rivers. Earth Surface Processes and Landforms, 2020, 45 (14), pp.3714-3731. 10.1002/esp.4996 . insu-02932260

HAL Id: insu-02932260

https://insu.hal.science/insu-02932260

Submitted on 7 Sep 2020

HAL is a multi-disciplinary open access archive for the deposit and dissemination of scientific research documents, whether they are published or not. The documents may come from teaching and research institutions in France or abroad, or from public or private research centers.

L'archive ouverte pluridisciplinaire **HAL**, est destinée au dépôt et à la diffusion de documents scientifiques de niveau recherche, publiés ou non, émanant des établissements d'enseignement et de recherche français ou étrangers, des laboratoires publics ou privés.



Distributed under a Creative Commons Attribution 4.0 International License

Check for updates

Baynes Edwin (Orcid ID: 0000-0002-8666-7628)

Sediment flux driven channel geometry adjustment of bedrock and mixed gravel-bedrock rivers

Edwin R.C. Baynes[1, 2, 3] *, Dimitri Lague[1], Philippe Steer[1], Stéphane Bonnet[4], Luc Illien[1, a]

[1] Univ Rennes, CNRS, Géosciences Rennes - UMR 6118, 35000 Rennes, France

[2] Department of Civil and Environmental Engineering, University of Auckland, Auckland, New Zealand

[3] Geography and Environment, Loughborough University, Loughborough, United Kingdom

[4] GET, Université de Toulouse, CNRS, IRD, UPS(Toulouse), France

[a] Now at: GFZ German Research Centre for Geosciences, Telegrafenberg, Potsdam, Germany

*Corresponding author email address: e.baynes@lboro.ac.uk

Running Head: Sediment flux driven channel geometry adjustment

This article has been accepted for publication and undergone full peer review but has not been through the copyediting, typesetting, pagination and proofreading process which may lead to differences between this version and the Version of Record. Please cite this article as doi: 10.1002/esp.4996

This article is protected by copyright. All rights reserved.

Accepted Article

Abstract

Sediment supply (Q_s) is often overlooked in modelling studies of landscape evolution, despite sediment playing a key role in the physical processes that drive erosion and sedimentation in river channels. Here, we show the direct impact of the supply of coarse-grained, hard, sediment on the geometry of bedrock channels from the Rangitikei river, New Zealand. Channels receiving a coarse bedload sediment supply are systematically (up to an order of magnitude) wider than channels with no bedload sediment input for a given discharge. We also present physical model experiments of a bedrock river channel with a fixed water discharge (1.5 l/min) under different Q_s (between 0 and 20 g/l) that allow the quantification of the role of sediment in setting the width and slope of channels and the distribution of shear stress within channels. The addition of bedload sediment increases the width, slope, and width-to-depth ratio of the channels, and increasing sediment loads promote emerging complexity in channel morphology and shear stress distributions. Channels with low Q_s are characterised by simple in-channel morphologies with a uniform distribution of shear stress within the channel while channels with high Q_s are characterised by dynamic channels with multiple active threads and a non-uniform distribution of shear stress. We compare bedrock channel geometries from the Rangitikei and the experiments to alluvial channels and demonstrate that the behaviour is similar, with a transition from single thread and uniform channels to multiple threads occurring when bedload sediment is present. In the experimental bedrock channels, this threshold Q_s is when the input sediment supply exceeds the transport capacity of the channel. Caution is required when using the channel geometry to reconstruct past environmental conditions or to invert for tectonic uplift

This article is protected by copyright. All rights reserved.

rates, because multiple configurations of channel geometry can exist for a given discharge, solely due to input Q_s.

Keywords: *Rivers, Bedrock, Sediment, Channel geometry, Physical modelling*

1. Introduction

The understanding of the processes that set the morphology of bedrock river channels, and the feedbacks and interactions that drive their evolution are crucial to develop a detailed understanding of rapidly evolving landscapes (Whipple, 2001; Turowski et al., 2006; DiBiase et al., 2015). The elevation of the river channel acts as the local base level for adjoining hillslopes. Vertical and lateral bedrock channel dynamics directly impact the hillslope sediment flux, through processes such as bank erosion and the undermining of hillslopes, and associated geohazards such as landsliding (Golly et al., 2017). In response to variations in climate or tectonic uplift rate, it has been shown that bedrock channels evolve dynamically through adjustments to both width and slope. This was observed across contrasting settings, including Nepal (Lavé and Avouac, 2001), California (Duvall et al., 2004), Italy (Whittaker et al., 2007), Taiwan (Yanites et al., 2010) and Scotland (Whitbread et al., 2015), as well as in experiments (Turowski et al., 2006) and predicted by mechanistic numerical modelling approaches (e.g., Stark, 2006; Turowski et al., 2007; 2008; Lague, 2010; Yanites and Tucker, 2010; Nelson and Seminara, 2011; Turowski, 2018; Li et al., 2020). However, landscape evolution models often assume that channel width scales simply with water discharge (Q) or drainage area (e.g. Whipple and Tucker, 1999; Shobe et al., 2017) or with a constant ratio between the channel width and channel depth (e.g., Finnegan et al., 2005), failing to capture

This article is protected by copyright. All rights reserved.

dynamic patterns of channel geometry identified in the settings above. This restricts the applicability of these models to account for changes in channel geometry due to climate or tectonic forcing that are important for setting river sediment transport capacity (Q_{sc}) (Croissant et al., 2017), bank erosion (e.g., Turowski et al., 2008), channel sinuosity (Stark, 2006; Turowski, 2018) and the undermining or stabilisation, in the case of channel narrowing, of adjoining hillslopes (e.g., Golly et al., 2017).

The key factors in setting the pattern and rate of erosion and the resulting morphology of bedrock river channels include the strength of the bedrock material (e.g. Montgomery and Gran, 2001; Yanites et al., 2017; Baynes et al., 2018a), sediment availability, or 'tools', for erosion by abrasion (e.g. Sklar and Dietrich, 2004, Turowski et al. 2007; Lamb et al., 2008; Cook et al., 2013; 2014; Brocard et al., 2016), the proportion of bedrock exposed on the bed, or the 'cover effect' (e.g., Turowski et al., 2007; Chatanantavet and Parker, 2008; Johnson et al., 2009; Lague, 2010), the degree of rock fracturing that promotes erosion by plucking or block toppling (e.g., Dubinski and Wohl, 2013; Lamb and Dietrich, 2009) and the magnitude and frequency of flood events (e.g., Hartshorn et al., 2002; Baynes et al., 2015). Of these factors, recent work has focussed on the processes driving vertical incision and the resulting channel geometries by sediment impacts, including the relative importance of suspended and bedload sediment (Scheingross et al., 2014) and the role of bed roughness and sediment flux (Finnegan et al., 2007; Johnson and Whipple, 2007; 2010). It has been observed, first by Gilbert (1877), and many times subsequently in the field (e.g., Sklar and Dietrich, 2001; Turowski et al., 2007; Johnson et al., 2009; Whitbread et al., 2015) and in laboratory experiments (e.g., Baynes et al., 2018b), that high sediment supply relative to river transport capacity can protect the bed from vertical incision (Turowski et al., 2013), with potentially

This article is protected by copyright. All rights reserved.

increased lateral erosion rates as a result of sediment impacts being more focussed on the channel banks (Turowski et al., 2008; Beer et al., 2017). Both the availability and nature (i.e., grain size) of bedload sediment that acts as 'tools' are important for controlling rates of erosion through abrasion in controlled experiments (e.g., Sklar and Dietrich, 2001) but the related impact on channel morphology remains relatively understudied. Finnegan et al (2017) identified the impact of grain size and sediment supply on steady-state bedrock channel slopes in a small (30 km^2) catchment in the Santa Cruz Mountains (California, USA). Tributary channels are three times steeper for a given drainage area where they transport coarse bedload but the main channel widens, shallows and shifts to more complete alluvial cover downstream of where it starts to transport coarse bed load material (Finnegan et al., 2017). In fully-alluvial channels, increasing sediment supply (Q_s) is crucial in setting the channel geometry and planform morphology, including an increase in width above that predicted by threshold theory (Lacey, 1930; Glover and Florey, 1951; Parker et al., 2007; Phillips and Jerolmack, 2016) and the transition to a braided river pattern at high Q_s compared to Q_{sc} (see review in Métivier et al., 2017). However, there remain outstanding questions on the link between Q_s, vertical and lateral erosion rate and the channel geometry (width and slope) in bedrock and mixed bedrock-gravel bed rivers across multiple scales (Turowski et al., 2007; Yanites and Tucker, 2010; Turowski, 2018; Lague, 2014; Finnegan et al., 2017), and how they respond to changes in Q_s (Turowski and Hodge, 2017; Yanites, 2018).

This study presents a combined field and experimental study to explore outstanding questions related to (i) the relationship between bedrock and mixed gravel-bedrock channel morphology (width and slope) and bedload sediment availability, and (ii) the morphodynamic processes that drive bedrock and mixed gravel-bedrock river

This article is protected by copyright. All rights reserved.

channel evolution under different sediment supply regimes. To answer these questions, we first explore trends in channel geometry of river channels in the Rangitikei catchment (~3000 km ^{2}) of the North Island of New Zealand, a natural laboratory where the impact of bedload sediment availability on channel geometry can be isolated and the nature of the bedload measured. We then use a physical model coupled with a numerical hydrodynamic model to explore the processes and interactions between sediment dynamics and channel incision in a controlled laboratory setting, allowing the processes leading to small changes in channel geometry to be identified and quantified. In particular we focus on the impact of bed cover on lateral erosion and the changing distribution of shear stress within channels under different sediment supply regimes.

2. Rangitikei River Catchment, New Zealand

2.1 Geomorphological setting

The channel geometry dataset presented here is from the Rangitikei river and surrounding catchments located in the central southern part of the North Island of New Zealand (Fig. 1). The rivers are, at present, incised bedrock and mixed gravel-bedrock channels, with a geomorphological history characterised by climatically-controlled cycles of aggradation and incision. The modern-day trunk channel of the Rangitikei is deeply incised into a strath terrace, topped by fluvial deposits, that was abandoned following the Last Glacial Maximum (Milne, 1973; Pillans et al., 1993; Litchfield and Rieser, 2005, Bonnet et al., 2019). In the middle reach of the Rangitikei river, the dating of recent terraces formed during post-LGM incision indicate a recent (post 10 kyr) incision rate of 1.5-2.0 mm/yr (Bonnet et al., 2019).

This article is protected by copyright. All rights reserved.

Importantly, for the purposes of this study, much of the trunk valley network is incised into weak Plio-Pleistocene marine mudstones to sandstones of the Whanganui Basin (Proust et al., 2005), but the lithology of the headwater regions has a strong spatial variation (Fig. 1). The eastern headwaters drain the Ruahine mountain range, supplying metamorphosed Triassic to early Cretaceous greywacke material as coarse bedload sediment to the river network while, in contrast, western headwaters have a very limited supply of such material due to lithological composition of these areas (Fig. 1). Therefore, due to the uniform weak lithology in the trunk channels, which are fed by tributaries both with and without a supply of coarse bedload sediment, the Rangitikei catchment is a natural laboratory where the role of bedload sediment supply in setting channel geometry can be assessed directly.

2.2 Methods

2.2.1 Channel geometry and drainage area

Measurements of the active channel width were collected from across the catchment using DigitalGlobe imagery in Google Earth (resolution 0.5 m). Measurements were collected from the trunk channel and tributaries both with and without a supply of coarse-grained bedload material from headwaters containing greywacke, to cover the full variability in channel geometry across the Rangitikei catchment (Fig. 1). All measurements of width were taken from locations where the local lithology is either sandstone or mudstone (Fig. 1) and were measured orthogonally to the river flow direction at distances of approximately 1 km. Measurements were made, as far as was possible, from straight channel reaches rather than the apex of meander bends to minimise the natural variability in the dataset. Active width was defined in the images as the distance orthogonal to the flow direction between either bedrock

This article is protected by copyright. All rights reserved.

banks (i.e., cliffs) or the limit of vegetated bars on the edge of the channels, to avoid uncertainty introduced by using the extent of the water coverage on the imagery. Where channels were multithreaded, the width measurement did not include the width of vegetated islands between channel threads. To test the level of natural variability in the channel width, 50 measurements were taken along a 500 m reach at Mangaweka, upstream of a large meander bend (Fig. 2F; 39.80932° S, 175.80811° E). The mean channel width from these measurements was 62.8 m with a standard deviation of 3.2 m, giving an uncertainty of approximately 5% in the width measurements as a result of the natural variability of the channel. Uncertainty related to human measurement error and the resolution of the Google Earth imagery was estimated by measuring the channel width in the same location within this reach 20 times, with a mean measurement of 63.8 m and a standard deviation of 1.2 m (~1.8%).

From each of the width measurements, upstream drainage area was extracted using a 90 m resolution Digital Elevation Model from the Shuttle Radar Topography Mission (SRTM) using the *r.water.outlet* tool in QGIS version 2.18. The lithology of the upstream drainage area was extracted for each of the width measurements using the geological map (Lee et al., 2011; Heron, 2014), and the percentage of the catchment draining basement greywacke rock used as a proxy for the supply of hard coarse-grained material.

2.2.2 Rainfall and river discharge

Drainage area at each location was converted to mean daily discharge, to remove any regional orographic rainfall control in the relationship between channel width and drainage area. Based on the difference between average annual rainfall from four

This article is protected by copyright. All rights reserved.

stations at high elevations in the Ruahine range and nine stations in the main catchment (see Supplementary Table 1 for annual rainfall data from locations across the catchment; provided by Horizons Regional Council), we identified an orographic rainfall pattern with a ratio of 1:1.54 between the western edge of the study area and the eastern limit of the measurements on the western side of the Ruahine range. To convert the drainage area to mean daily discharge (Q_m) for the western catchments, we assumed the orographic rainfall increased at a constant rate from west to east and used the following equation:

$$Q_m = R \times K \times A$$

Where *R* is the value of the orographic rainfall value between 1 and 1.54 as a function of the relative distance from the measurement location between the western edge of the study and the location of peak rainfall, *A* is the catchment drainage area and *K* is the scaling constant between drainage area and mean daily discharge calculated using the discharge record from the gauging station at Mangaweka (39.80932°S, 175.80811°E):

$$K = \frac{Q_{Mangaweka}}{R_{Mangaweka} \times A_{Mangaweka}}$$

For the three catchments located to the east of the Ruahine, in the absence of any rainfall data, we assumed a decrease in the orographic rainfall pattern of 1.54:1 from the peak rainfall location used above to the eastern limit of the study area and calculated the mean discharge for each location according to the relative position along this orographic gradient.

This article is protected by copyright. All rights reserved.

2.2.3 Sediment grain size distribution

The catchment wide channel geometry and catchment lithology data was supplemented with field measurements of sediment grain size at locations across the catchment where sediment was stored within the channel and easily accessible for measurement (Fig. 1). A random walk method of sampling the a-axis of 125 grains along a 20 m transect was performed at each location (Wohl et al., 1996). Multiple transects at the same location were collected where clear spatial differences in grain size were apparent on active bars within the channel compared to bars on the channel banks (see SI Section 2 for details of number of transects per site, and photos of the sites).

2.3 Field data

2.3.1 Channel width

The presence of hard, coarse-grained, bedload sediment is clear within the channels that drain part of the Ruahine mountain range (Fig. 2). These channels are wider than channels that do not receive a supply of coarse-grained bedload material from the headwaters (Fig. 2A-C). The width of the Kawhatau river (Fig. 2D) is an order of magnitude greater than the Makohine river (Fig. 2A), despite having a drainage area only three times greater and flowing through similar weak lithology.

Analysis of the catchment wide channel width dataset (Fig. 3A; Table 1) demonstrates that the channel width increases with discharge, consistent with observations from other natural settings (e.g., Lague, 2014). There is also a clear relationship between channel width and whether the catchment drains areas of greywacke lithology, used as a proxy here for coarse-grained bedload sediment. Channels that do not drain any greywacke (in white in Fig. 3A) are systematically

This article is protected by copyright. All rights reserved.

narrower than channels that do have a supply of coarse bedload sediment from the headwaters (shades of grey/black in Fig. 3A) across two orders of magnitude variation in mean daily discharge. Normalisation of the channel width by $Q^{0.5}$ (the common scaling for bedrock channels reported in the literature; see Lague, 2014) further demonstrates a dependency between the channel width and the proportion of the catchment supplying coarse sediment (Fig. 3B). Further analysis of normalised channel width according to the proportion of the upstream catchment that drains greywacke (Fig. 3C) also highlights the role of bedload sediment supply on the channel morphology with normalised channel width broadly increasing in a linear relationship (r^2 = 0.48, p-value = 0.009). Channels without a bedload supply have very low normalised channel widths (~ 0.01) while channels with a supply of coarse bedload sediment have normalised channel widths ranging from 0.02 to 0.09. The relationship between the coarse bedload sediment supply and the channel width is most prominent in small tributaries close to the Ruahine range front where a larger upstream proportion of the catchment is greywacke (mean daily discharge between 0.5 and 10 $m^3 s^{-1}$) compared to the trunk channel where the discharge is largest (> 50 $m^3 s^{-1}$) and the normalised channel widths are generally lower (Fig. 3B,C).

2.3.2 Grain size

We have investigated how the grain size varies with transport distance rather than the catchment drainage area due to the spatially variable nature of the bedload sediment supply into the headwater tributaries. For example, the drainage area of the Rangitikei (stars in Fig. 4A) increases threefold between the upstream and downstream locations (Table S1), but there is not a coincident increase in supplied sediment volume as the majority of the additional tributaries do not drain the source of the greywacke sediment; the Ruahine mountain range (Fig. 1). The transport

This article is protected by copyright. All rights reserved.

distance is therefore a more representative parameter in this setting for exploring sediment grain size variability and any possible impact of the grain size on the channel geometry within the study catchments. Transport distance was measured as the longitudinal distance between the edge of the greywacke areas to the grain size measurement site (Fig. 1). Where multiple tributaries drain the greywacke (e.g., in the Rangitikei, downstream of the confluence with the Kawhatau; Fig. 1), we used the shortest transport distance to the greywacke contact but the transport distance from the greywacke contact along the trunk channel is also provided in Table S2.

Other than a single outlying transect from the Pohangina river, there is no clear trend of downstream fining of the median (D_{50}) or coarsest (D_{90}) sediment grain size fractions over a transport distance of up to 70 km from the Ruahine mountain range. The D_{90} is consistently between ~100-300 mm (Fig. 4). The outlying transect of the Pohangina (D_{90} = 510 mm) was measured from the outside of a meander bend near a bridge, and the D_{90} from another transect measured from a gravel bar in the middle of the active channel at the same location (40.05237° S, 175.93847° E) was 153 mm. While it wasn't the only survey site with a nearby bridge, we suggest the local conditions of the outlying transect on the outer meander bend immediately downstream of the bridge pile have led to a non-representative grain size from this location and we do not consider this transect further. Given the relatively consistent grain size across the catchments located close (< 25 km) to the Ruahine range front, which typically have low mean daily discharge (Table S2), we suggest that variations in the sediment grain size cannot solely be the cause of the large variability in normalised channel width (between 0.02 – 0.09; Fig. 4B) for these rivers.

In the trunk channel of the Rangitikei, there is no clear downstream fining trend in the coarse fraction of the sediment grain size distribution (Fig. 4A). The normalised

This article is protected by copyright. All rights reserved.

channel widths in the Rangitikei are typically lower than the catchments close to the mountain range front despite a similar proportion of the catchment draining greywacke (normalised channel width ~0.01-0.02; Fig. 4B), possibly the result of the slightly smaller grain size in the trunk channel. However, the trend in the sediment grain size data is not strong enough to suggest that the variability in the normalised channel width with discharge is solely the result of sediment grain size variability within the channels (Fig. 4B).

3. Physical modelling of the impact of sediment flux on channel geometry

The results from the Rangitikei River clearly demonstrate that bedload sediment flux has a significant impact on the channel geometry at the catchment scale but is limited by the lack of data showing the dynamics of channel geometry variability at the reach scale. Here, we complement the data from the Rangitikei with a suite of controlled laboratory experiments performed at the reach scale, allowing additional data to be collected related to the impact of sediment flux on the hydraulics within the channel (e.g., shear stress) and also to be able to monitor the evolution of the channel slope.

3.1 Experimental approach

3.1.1 Flume set up

Analogue physical model experiments were performed in the 80 cm x 30 cm Bedrock River Experimental Incision Tank at Université de Rennes 1 (Fig. 5; see Turowski et al., 2005; 2006; Turowski, 2007; Baynes et al., 2018a; 2018b for more information on experimental apparatus). While no formal scaling of the experiments with a particular natural location was sought, the similarity of the processes represented in the

This article is protected by copyright. All rights reserved.

analogue model allow the exploration of the impact of different boundary conditions on channel morphology and the evolution of the system over spatial and temporal scales that would otherwise be impossible using strict scaling approaches (Hooke, 1968, Paola et al., 2009; Baynes et al., 2018c). The experiments were designed to isolate the role of sediment flux (Q_s) on bedrock channel geometry in a tectonically quiescent setting and identify the processes that explain the observations of channel geometry in natural rivers. Seven experiments (Table 2) were performed under a constant water discharge using a mix of homogenous cohesive silica material (grain size = 45 µm) with uniform strength (Baynes et al., 2018a). During an initial channel adjustment phase, the channel outlet was dropped by 2 cm to generate a knickpoint that formed an incised channel with cohesive 'bedrock' banks rather than unchannelised flow over a flat surface. Following this initial base level fall to channelize the flow, the elevation of the channel outlet was fixed throughout the rest of the experiment. Channel geometry has been shown to be a function of the tectonic uplift rate (e.g., Lavé and Avouac, 2001; Duvall et al., 2004; Whittaker et al., 2007), but is not considered in the experiments presented here as the channel outlet elevation was fixed following the initial channelization phase. The experiments therefore represent a different type of tectonic setting to many existing studies, where the role of tectonics in controlling channel geometry is a main focus (e.g., Turowski et al., 2006). To represent bedload sediment material, coarse sand (grain size = 250 µm) was added at the channel inlet using a Gericke Infinite Screw feeder system. The sand was collected beyond the channel outlet to avoid any deposition in the channel as a result of the channel outlet configuration (Fig. 5). The channel width and slope were free to adjust in response to the Q_s through lateral erosion of the

This article is protected by copyright. All rights reserved.

banks, or deposition of material or erosion of the channel bed when exposed to clear water flow.

Channel geometry evolution during the experiments was monitored using a Leica ScanStation 2 terrestrial laser scanner, programmed to collect high resolution (sub-mm) point clouds of the topography every two minutes. The ScanStation 2 uses a green laser that penetrates water. The point clouds were gridded to generate Digital Elevation Models (DEMs) at 2 mm resolution, and the resulting DEMs were used as input for the *Floodos* numerical hydrodynamic model (Davy et al., 2017). The *Floodos* model generates a water depth map over the topography for a given discharge, which was used to automatically extract channel geometry information as well as calculate hydraulic information such as bed shear stress or Froude number (see Baynes et al., 2018b for further description of the *Floodos* model parameter calibration for predicting hydraulic information in the experimental channels).

3.1.2 Relevance of laboratory experiments to the Rangitikei catchment

Direct comparison of the laboratory results to particular locations within the Rangitikei study area are limited. Instead, the experiment is designed to replicate the key behaviour of the target system, allowing the spatial and temporal scales to be reduced, and allowing greater flexibility in a range of parameters to be tested. There is a key difference between the dominant erosion process in the Rangitikei (abrasion) and the experiments (hydraulic shear by clear water flow) negating the possible comparison of the 'tools effect' between the experimental results and the natural setting. However, we suggest that the other key ingredients of the experiments replicate the processes in the Rangitikei well: a weak bedrock material

This article is protected by copyright. All rights reserved.

that can be easily eroded by hydraulic shear (aided in the Rangitikei by wetting-drying cycles that weather the bedrock), and the coarse cover of sediment that can protect the channel bed from vertical incision, the 'cover effect' (Sklar and Dietrich, 2004; Turowski et al., 2007; Chatanantavet and Parker, 2008; Johnson et al., 2009; Lague, 2010). Despite the lack of the 'tools effect' in the experiments, we suggest that the important process for studying the effect of sediment supply of bedrock channel geometry is the cover effect, with channel widening occurring when the bed is protected from vertical erosion and flow is directed towards the channel walls (e.g., Turowski, 2018). We therefore acknowledge the limitations of the experimental approach for the lack of the 'tools effect' but suggest that the similarity of the other processes, particularly the presence of the 'cover effect' allows insights to be drawn on the role of sediment supply in setting the width and slope of bedrock channels.

3.2 Experimental results

3.2.1 Evolution of channel geometry

Channel width evolution through time during the experiments is shown in Figure 6, with the initial phase at the start of the experiment where the channelization of the flow took place highlighted in red. All subsequent reporting of results does not include this initial phase when the channel geometry is affected by the incisional nature of the channel as well as the input Q_s. It should be noted that the end of this initial phase does not necessarily indicate the time when the channel geometry has stabilised, but rather when the initial phase of channelization and generation of a bedrock constrained channel has been completed (i.e., the knickpoint has reached the channel inlet and the channel is fully channelized). At this time, the channel width is still adjusting to the balance of the input Q_s, including the reduction in supply of

This article is protected by copyright. All rights reserved.

material eroded from the bed (i.e., by the retreating knickpoint). The fluctuations in the channel width measurements can be estimated through the errorbars in Fig. 6, which indicate two standard deviations from the mean value of width of the cross-sections from each of the DEMs. For channels with low Q_s (Fig. 6A-C), the natural variability in the channel is low. The channels become more dynamic with increasing Q_s (e.g., Fig. 6D-G), due to the presence of a migrating channel thalweg and the generation of small terraces.

Figure 7 provides summary statistics for the channel geometry for all of the Digital Elevation Models (DEMs) during each experiment, excluding the channel initialisation phase (see Fig. 6). For example, the violin plot for Q_s = 0 g/l contains all of the channel geometry measurements from after the initial incision phase (t = 92 mins) until the end of the experiment (t = 240 minutes). The data was extracted from the whole channel reach, with the exception of the upper and lower 20 cm of the flume to negate any possible impact of the channel inlet and channel outlet. The width (W), slope (S) and width-depth ratio (W/D) of the experimental channels varies with the input Q_s (Fig. 7), with channels typically wider and steeper under higher Q_s. Q_s appears to have the largest impact on the channel slope, and the spread with the plots in Fig. 7 indicate the degree of variability in the W, S and W/D under the different sediment regimes. The median channel width and slope values at low Q_s are similar, but the wider spread of the channel widths at Q_s = 2.5 and 5 g/l compared to Q_s = 0 g/l indicates the impact on channel morphology. However, some of the extreme values that make the tails of the plots may be indicators of the state of the channel shortly after the initial channelization phase when the channel has not necessarily fully stabilised (Fig. 6).

This article is protected by copyright. All rights reserved.

3.2.2 Channel form at representative conditions

In addition to the impact on mean W, S and the W/D, Q_s also has an important role in setting the morphology and characteristic dynamics of the channels. To directly compare the results of typical channel geometry under the different Q_s regimes, we extracted data from individual DEMs that are representative of, or as close as possible to, channels that have fully evolved to the input Q_s. We define a channel as being 'representative' as the time when the channel geometry has had plenty of time to evolve to the input conditions and is not undergoing widespread changes (Fig. 6). The timing of the DEMs that we selected for each Q_s regime are shown by the blue lines in Fig. 6. Typically, these 'representative' conditions are at the end of the experiment, giving the full 240 minutes for the channel width and slope to stabilise to the input Q_s. The mean channel width data for each DEM presented in Fig. 6 indicates the temporal evolution of the channel through time and the standard deviation errorbars indicate the variability in the channel width for each DEM. Typically this variability is reduced as the channel stabilises through time (e.g., Fig 6A, B), but there is some variability in the width throughout the length of the experiments for the higher sediment fluxes. Under these conditions, we selected the DEM closest to the end of the experiment that appeared visually stable and did not contain any DEM artefacts generated during the interpolation process.

Given this continued small-degree of variability, we refer to these as 'representative' channels rather than 'steady-state' to reflect the potential for not having reached perfectly stable conditions, and also to avoid confusion with the common usage of the term 'steady-state' to refer to the balance between vertical erosion and uplift rate. Additionally, we chose to consider all the cross-sections for each DEM to demonstrate the natural variability in the channel width, rather than the temporal

This article is protected by copyright. All rights reserved.

evolution of a single cross-section which may not fully represent the channel morphology at any given time. However, we suggest that using the channel geometries from these extracted 'representative' times allows a better comparison between Q_s regimes than using data extracted from the entire time period including immediately after the initialisation phase (Fig. 6). Due to these limitations discussed above, we exercise caution when directly comparing the experimental results to the Rangitikei natural example, but we suggest that the experiments are still informative, showing the relative impact of Q_s on the channel geometry for a fixed discharge within the same system (from Q_s = 0 g/l to Q_s = 20 g/l).

The experiments with a low Q_s (0 and 2.5 g/l) were typically characterised by a single active channel, with a stable channel bed, and partial bed cover by sediment for 2.5 and 5 g/l (Fig. 8A-H; Fig. S8). The channels at higher Q_s deposited material on the whole channel bed, increasing the elevation of the channel bed and adjusting the channel slope (Fig. 7). It is important to note that during the Q_s = 20 g/l experiment, the banks of cohesive 'bedrock' were buried under by sediment deposited on the channel bed (Fig. 8M-N). This led to dynamic channels that migrated across the width of the flume, sometimes reaching the edges (e.g., Fig. 8M), and typically behaving more like an alluvial system rather than a bedrock or mixed gravel-bedrock channel. This experiment therefore represents a comparison dataset between the dynamics of an 'alluvial' channel and bedrock or mixed gravel-bedrock channels in the experimental setup.

Accepted Article

This article is protected by copyright. All rights reserved.

3.2.3 Bed shear-stress

In addition to the water depth mask (Fig. 8), the *Floodos* hydrodynamic model output (Davy et al., 2017) was used to calculate the bed shear stress for each pixel within the channels, $\tau = \rho g D S$, where τ is bed shear stress, ρ is density of water (1000 kg m^{-2}), D is the water depth and S is the hydraulic slope. The distribution of shear stress values within the channel at 'representative' conditions for each of the Q_s regimes is shown in Fig. 9. Typically, the mean and median τ within the channel across the different Q_s regimes is relatively similar, with all values above the critical shear stress (τ_c) (see below). For experiments where Q_s > 0 g/l, the range of τ values was greater than the Q_s = 0 g/l experiment, with a higher peak shear stress (τ_{max}) but also more values closer to 0 Pa (Fig. 9). From Figure 9, there is no apparent link between increasing Q_s and increasing τ for individual pixels within the channel, but due to variability in channel width (Figs. 7; 8) this does not necessarily mean that there is no increase in total sediment transport potential with higher Q_s. The critical shear stress (τ_c) was calculated using the following equation:

$$\tau_c = \tau_c^*(\rho_s - \rho_w) g D_{50}$$

Where τ_c^* is the Shield's criterion (typically 0.03 - 0.06; Buffington and Montgomery, 1997), ρ_s is the density of the sediment (2750 kg m^{-3}) , ρ_w is the density of water (1000 kg m^{-3}), g is the acceleration due to gravity (9.81 m s^{-2}) , and D_{50} is the median grain size of the sediment (250 μm). Using these values, we calculate τ_c to be ~0.15-0.25 Pa, approximately 3-4 times smaller than the mean and median τ (Fig. 9) which is a similar ratio to many natural gravel-bedded rivers such as those located in western North America (Pfeiffer et al., 2017). Following Meyer-Peter and Muller (1948) and Lajeunesse et al. (2010), we compute the 'excess bedload shear stress'

This article is protected by copyright. All rights reserved.

(τ_{bl}), for each pixel during the representative width conditions to explore the potential for sediment transport within the channel:

$$\tau_{bl} = \frac{(\tau - \tau_c)^{\frac{3}{2}}}{\tau_c}$$

We calculated τ_{bl} for each pixel within the studied reach of the experiments, and extracted the cumulative τ_{bl} across twenty channel cross-sections at equal intervals (18 mm) from the studied reach (see Fig. 8 for excluded areas at channel inlet and outlet). A higher cumulative τ_{bl} within the channel indicates a greater potential for sediment transport, as there are more pixels where the $\tau > \tau_c$. The mean total τ_{bl} (across 20 cross-sections) increases with Q_s when Q_s > 5 g/l (Fig. 10) under a range of τ_c values (0.1 - 0.3), to take into account a range of values for the Shield's criterion discussed above. Where $Q_s \leq 5$ g/l, the total τ_{bl} is approximately the same for all of the experiments.

3.2.4 Sediment flux, bed shear-stress and river lateral mobility

Importantly, despite an increase in τ_{bl} with increasing Q_s, the distribution of τ on the channel bed does not follow the same pattern for each Q_s regime (Fig. 9; 11). For each experiment, the two columns of Figure 11A show examples of two DEMs, with the twenty cross-sections plotted next to each other (same cross-sections used for the τ_{bl} calculation in Fig. 10). The normalised shear stress at a single point (τ/τ_{max}) is coloured at each location along the cross-section. Probability density functions (pdf) of τ/τ_{max} across the cross-sections are shown in Fig. 11B for the first two DEMs as well as three additional DEMs. Where τ is close to being uniformly distributed across the width of the channel, τ/τ_{max} in a cross-section would all be

This article is protected by copyright. All rights reserved.

close to 1 (darker colours in Fig. 11A and the pdf shows that most values lie towards high values of τ/τ_{max}). Where τ is distributed unevenly, there would be sections of the cross-section where τ/τ_{max} is close to 1, and other areas where τ/τ_{max} is close to zero (lighter colours in Fig. 11A and a probability density function dominated by values that lie close to low values of τ/τ_{max}).

Where Q_s = 0 g/l, τ is distributed uniformly across the whole width of the channel, and the planform morphology is stable through time (e.g., the top row of Fig. 11; and the small range of values in Fig. 9). When Q_s > 0 g/l, the distribution of τ/τ_{max} becomes increasingly complex with a network of 'active' channel threads that contain higher τ than other parts of the cross-section, shown by the pattern of light and dark patterns in the bottom panels of Fig. 11. Additionally, the pdfs show that with an input Q_s, the shape of the curve shifts such that more values lie towards a low value of τ/τ_{max}. At Q_s = 0 g/l, there is unimodal peak with a relatively narrow standard deviation centred at τ/τ_{max} ~ 0.75, while at Q_s = 2.5, 6.66 and 7.5 g/l a broader peak is centred at τ/τ_{max} ~ 0.5. At Q_s = 10, 20 and, to some extent, 5 g/l, there is a general decay in the frequency of high τ/τ_{max}, indicating that the majority of the channel does not have a τ close to τ_{max}. At Q_s = 20 g/l, where the channel is alluvial in nature, the distribution of τ is dynamic and evolves quickly through time (see the difference in the spatial map of τ/τ_{max} in the bottom panels of Fig. 11 showing DEMs that are separated by two minutes). Therefore, under high Q_s, the channel morphology evolves to accommodate the extra material but the sediment transport does not occur at a uniform rate across the whole width of the channel. A similar behaviour can be seen, to a lesser extent, for Q_s = 7.5 and 10 g/l suggesting that mixed bedrock-gravel channels, with cohesive 'bedrock' banks, are also dynamic systems that evolve their morphology according to the input Q_s.

This article is protected by copyright. All rights reserved.

4. Discussion

4.1 Comparison to theoretical predictions of channel geometry

4.1.1 Constant width-depth ratio

Finnegan et al. (2005) proposed, on the basis of Manning's formula, that river width is a function of the lithology into which the channel is developed, with a constant ratio between the width and the depth for a given substrate. The experimental results presented here (Fig. 7) demonstrate that the W/D can be highly variable, as a function of Q_s. Therefore, we suggest that while the use of a constant W/D for the modelling of bedrock channel width gives a first order estimate of the channel geometry through the consideration of the role of discharge, this simple approach fails to capture the impact of the complexities of erosion-sedimentation processes. In particular, the experiments highlight the role of sediment cover on the bed favouring erosion of the channel banks that, in turn, drives increased rates of lateral erosion and channel widening (e.g., Turowski et al., 2009; Turowski, 2018; 2020; Li et al.; 2020). This behaviour is consistent with observations from Boulder Creek, California, USA, where the main channel was wider and shallower downstream of the introduction of coarse bedload material (Finnegan et al., 2017).

4.1.2 Threshold theory

According to Lacey's law (Lacey, 1930; Glover and Florey, 1951; Métivier et al., 2017), when the conditions within a channel are just above the threshold for entrainment of the sediment, the channel geometry (width and slope) is set by the balance between gravity and fluid friction, and the width scales with the square root of the discharge:

This article is protected by copyright. All rights reserved.

$$\frac{W}{D_{50}} = \left[\frac{\pi}{\sqrt{\mu}}\left(\frac{\theta_t(\rho_s-\rho)}{\rho}\right)^{-\frac{1}{4}}\sqrt{\frac{3C_f}{2^{\frac{3}{2}}\,\mathrm{K}\left[\frac{1}{2}\right]}}\right]Q_*^{\frac{1}{2}}$$

Where μ is the friction angle, θ_t is the threshold Shield's parameter, C_f is the turbulent friction coefficient, $\mathrm{K}\left[\frac{1}{2}\right]$ is a transcendental integral with value of ~1.86 and $Q_* = Q/\sqrt{gD_{50}^5}$ (Glover and Florey, 1951; Métivier et al., 2017). The width of channels normalised by the sediment grain size in the Rangitikei are typically larger than the width predicted by the Lacey relationship for channels at the threshold for entrainment for the corresponding discharge and sediment grain size (Fig. 12). Note that in this analysis we use three different scaling factors between bankfull discharge (Q_{bf}) and the mean daily discharge (Q_m). In SI Section 3, we estimate based on analysis of gauge data and a survey of river stage that $Q_{bf} = 4.5\,Q_m$ (Fig. 12B) for the Rangitikei but we provide the other plots to demonstrate the impact of the Q_{bf} scaling factor on Q_*. For the experimental channel, the grain size used (D_{50}), when Q_s = 0, 2.5 and 5g/l, where the bed was not or only partially covered, was 45 µm (for the silica 'bedrock' material). For all other experiments, the grain size used was 250 µm (for the sand). The choice of D_{50} is important for the calculation of Q_* and W/D_{50} and is why the channels with low Q_s have larger values of Q_* and W/D_{50} in Fig. 12 than channels where Q_s > 5 g/l. Despite this, it is still possible to compare the relative difference between observed W/D_{50} for the experimental channels with the predictions of Lacey's law (Fig. 12).

Using an extensive compilation of previous experiments of alluvial channels Métivier et al. (2017) found a relationship of increasing channel width with Q_s before a transition in channel morphology from single thread to braided river conditions

This article is protected by copyright. All rights reserved.

occurs. In this compilation, single thread channels typically have a lower Q_s, and the width is closer to the threshold width predicted by Lacey's law (Fig. 12). A similar relationship is found in the experimental data in this study and data from Baynes et al. (2018a) experiments without Q_s but at variable discharge. Experiments in Baynes et al. (2018a) are close to the predicted width at threshold for entrainment conditions, while the experiments in this study with an input Q_s plot further from threshold theory (Fig. 12). Differences in the channel geometry from a clear single thread to a more variable channel planform with increasing Q_s is also observed in the Rangitikei (Fig. 3), in other field locations that contain strath terraces where narrower channels have incised within wider braid plains following reductions in sediment supply (e.g., Finnegan and Balco, 2013), and in our experiments (Fig. 8; 11), although a threshold Q_s where this behaviour begins is hard to identify beyond being in the region of 5-7.5 g/l. Importantly, despite the experiments in this study being performed with cohesive bed material, they follow the same pattern of a transition to different planform morphologies and distribution of shear stress at very high Q_s. The sensitivity of Q_* to the Q_{bf} scaling factor controls how aligned the Rangitikei channels are to the compilation dataset of Métivier et al. (2017) and threshold theory, but does not impact the pattern within the Rangitikei dataset, where channels with a higher bedload sediment supply typically plot further from the threshold theory and can experience a change in the channel behaviour (e.g., Fig. 2). We therefore suggest that Q_s dependent channel form is not just a feature of alluvial rivers typically considered in the compilation of Métivier et al. (2017), but also rivers constrained by banks made of relatively weak bedrock material (e.g., the mudstone of the Rangitikei or the experimental substrate).

This article is protected by copyright. All rights reserved.

4.2 Adaptation of channel geometry and bed shear stress in response to sediment flux

Figure 13 demonstrates the range of possible channel geometry configurations (i.e., W and S) at a constant discharge under different Q_s. For comparison, we have included a reference dataset from similar experiments, where $Q_s = 0$ but under different discharges (from Baynes et al., 2018a). For a constant discharge, the impact of Q_s on the width and slope of channels is greater than the impact of changing the discharge when $Q_s = 0$ g/l, with the variability in the Q_s dataset larger than the reference dataset that covers an order of magnitude of discharges (Fig. 13). Here we explore the processes that could explain the geometric adaptation to these different Q_s scenarios, linking back to the Rangitikei.

When Q_s is low, the characteristic bedrock channel conditions are detachment-limited and bedrock erosion processes dominate the evolution of the channel geometry (Lague, 2010). For an incising channel under detachment-limited conditions, the channel geometry is set by the incision rate and independent of Q_s (Lague, 2010). In our experimental channels where incision rate (I) = 0 and $Q_s = 0$, channel geometry is dependent on the τ_c and there is a uniform distribution of τ_{bl} within the channel (Figs. 10; 11). A small increase of Q_s (2.5 and 5 g/l) does not seem to drive an increase in τ_{bl} (Fig. 10) suggesting that the channel transport capacity (Q_{sc}) was higher or equal to 5 g/l.

For $Q_s > 5$ g/l, the channels widen and steepen to increase their transport capacity. By definition, if a channel changes its geometry to accommodate an increase in sediment supply, it is no longer under detachment-limited conditions (e.g., Lague, 2010). The channel can then evolve towards strict transport-limited conditions ($Q_s = Q_{sc}$) or hybrid conditions ($Q_s < Q_{sc}$) (Lague, 2010) for which the geometry is set by a

This article is protected by copyright. All rights reserved.

combination of the upstream Q_s and local incision rate. Because I = 0 in our experimental setup and the discharge is constant, the fraction of the bed covered by sediment is an indirect indication of these conditions: if the channel bed is fully covered by sediment, and in particular with a thick immobile sediment cover, it is under transport-limited conditions. If the bed is only partially covered with immobile sediment, this means that the local Q_s is equal or larger than the local Q_{sc}, but the complete channel section could be in hybrid or transport-limited conditions ($Q_s \leq Q_{sc}$). This is specific to the experimental configuration for which discharge is constant. In natural rivers, the analysis of the long-term conditions of mixed bedrock-alluvial channels based on the present-day sediment cover at low flow is more difficult owing to stochastic fluctuations in discharge and sediment supply (Lague, 2010). At 'representative width' conditions, the experimental channel was fully covered with sediment when $Q_s \geq 6.66$ g/l, with partial bed coverage for $Q_s = 2.5$ and 5 g/l (Fig. S8), suggesting that it is very likely that the experimental channel transitions to transport limited conditions when $Q_s > 5$ g/l.

Under constant discharge conditions, wider channels would decrease the τ as the flow is spread over a larger wetted area and thus has a reduced water depth. However, the coincident increase in the channel slope (Figs. 7; 13) as well as the morphodynamic transition towards an actively migrating braided system of narrow threads with high local τ (Fig. 11) contribute to the overall increase of channel transport capacity. This behaviour of the experimental bedrock-gravel channels appears consistent with the behaviour and characteristic morphology of alluvial rivers. The presence of an input Q_s leads to a larger offset from the theoretical predictions of Lacey's Law (Fig. 12) and the transition from single thread to multiple

This article is protected by copyright. All rights reserved.

threaded channels after reaching a threshold sediment supply and shift to transport limited conditions (Q_s > 5 g/l).

4.3 Geometry of the rivers in the Rangitikei region

The scaling between width and discharge for most of the channels in the study area (Table 1) follows the common relationship found in bedrock rivers across multiple settings ($W = kQ^{0.5}$, where k is a constant; Lague, 2014). However, three of the channels (Hautapu, Pohangina, and Makaroro) are notable exceptions due to a negative exponent. The Pohangina (Fig. S6) and Makaroro both drain the Ruahine mountain range, are heavily laden with coarse sediment, and in-channel bars and multiple active threads are evident. We suggest the negative exponent in these channels may be related to the high sediment supply or local variabilities in lithological strength, especially in the Lower Pohangina, where the bedrock includes a thick succession of coarse terrigeneous clastic deposits (Rees et al., 2017). Further detailed field study of these channels would highlight these controls. The Hautapu contains no coarse sediment and close to the confluence with the Rangitikei trunk channel, the valley is more incised and narrower (Fig. 2C) than upstream (Fig. 2B). We therefore suggest that the general narrowing of the channel with discharge in the Hautapu is related to the response of the tributary to vertical incision in the Rangitikei, with the incision wave yet to fully migrate upstream. Despite these three exceptional channels, it is clear that the availability of bedload sediment has an important role on the bedrock channel width in the Rangitikei by affecting the magnitude of 'k' in the scaling between width and discharge (Table 1; Figs. 2; 3).

There exist two components to the 'tools' effect, (i) sediment availability and (ii) the nature of that sediment (i.e., grain size or lithology; Sklar and Dietrich, 2001). In the

This article is protected by copyright. All rights reserved.

Rangitikei, we suggest that sediment availability is the dominant component of the 'tools' effect as the sediment grain size is relatively consistent throughout the channels (Fig. 4). We propose that in the channels with a high availability of coarse-grained bedload, the 'cover' effect protects the bed from erosion and drives an increased volume of impacts on the channel banks, driving lateral erosion and widening the channel.

The transition from detachment-limited to transport-limited conditions and different behaviour of the channel system due to bedload sediment flux is evident in the example from the Rangitikei. Tributaries that do not receive a supply of coarse-grained bedload material represent the detachment-limited channel configuration for a given discharge (Fig. 2; 3), while any departure from this geometry due to coarse-grained bedload sediment supply represents a transport-limited or hybrid channel configuration. The channels that are not supplied with coarse grained bedload material from greywacke areas plot close to the threshold theory (Fig. 12), similar to the $Q_s = 0$ g/l experiments, while the tributaries that drain a high proportion of greywacke plot further from the threshold theory, consistent with channels that have a high bedload sediment flux (Fig. 12). These channels also actively migrate laterally (Lague et al., 2013; Bonnet et al., 2019) as a meandering bedrock channel, and sometimes contain multiple active threads (Fig. 2) whereas the channels with a low/no bedload sediment supply are more uniform in nature, consistent with the distribution of shear stress within the experimental channels where $Q_s = 0$ g/l (Fig. 11). We therefore suggest that the findings from the experiments, where channels become less uniform in terms of the value and distribution of shear stress after a transition to transport-limited or hybrid conditions, are applicable to natural environments such as the Rangitikei region.

This article is protected by copyright. All rights reserved.

5. Conclusion

Sediment is a critical component of bedrock channel systems, with the supply of hard, coarse-grained, material as bedload having a direct impact on the width of channels in the Rangitikei river, New Zealand. The presence of a bedload sediment supply acts to protect the channel bed from vertical erosion, increasing impacts on the channel banks and leading to increased channel widths for a given river discharge. Under experimental conditions, varying sediment supply leads to a range of possible configurations of channel width and slope for a given discharge. Increased sediment supply leads to a complex and evolving pattern of shear stress within the channel as the pattern of flow becomes more dynamic, while maintaining a constant mean shear stress just above the critical shear stress for the motion of sediment, replicating a similar effect identified in laboratory and natural alluvial channels. We therefore suggest that sediment flux should be an important parameter to consider when using preserved bedrock channel geometries to reconstruct past conditions (e.g., palaeo-discharge), or estimate uplift rates from channel geometry, as a range of possible configurations may be possible for a given discharge. The feedback between sediment supply and channel geometry should also be included in numerical models of landscape evolution. Further work is required to identify the response of bedrock channel geometries to variable sediment supply through time.

Accepted Article

This article is protected by copyright. All rights reserved.

References

Ashmore, P., 2013. Fluvial Geomorphology, in: Morphology and dynamics of braided rivers, vol. 9 of *Treatise on Geomorphology*, 289–312, Academic Press, San Diego, CA, USA

Baynes E.R.C., Attal M., Niedermann S., Kirstein L.A., Dugmore A.J., Naylor M., 2015. Erosion during extreme flood events dominates Holocene canyon evolution in northeast Iceland. *Proceedings of the National Academy of Sciences* 112 (8), 2355-2360. DOI: 10.1073/pnas.1415443112

Baynes, E.R.C., Lague, D., Attal, M., Gangloff, A., Kirstein, L.A., Dugmore, A. J., 2018a. River self-organisation inhibits discharge control on waterfall migration. *Scientific Reports* 8, 2444

Baynes, E.R.C., Lague, D., Kermarrec, J-J., 2018b. Supercritical river terraces generated by hydraulic and geomorphic interactions. *Geology* 46 (6), 499-502

Baynes, E.R.C., van de Lageweg, W.I., McLelland, S.J., Parsons, D.R., Aberle, J., Dijkstra, J., Henry, P-Y., Rice, S.P., Thom, M., Moulin, F., 2018c. Beyond equilibrium: Re-evaluating physical modelling of fluvial systems to represent climate changes. *Earth-Science Reviews,* 181, 82-97

Beer, A.R., Turowski, J.M., Kirchner, J.W., 2017. Spatial patterns of erosion in a bedrock gorge. *J Geophys Res. Earth Surf* 122, 191-214

Bonnet, S., Reimann, T., Wallinga, J. Lague, D., Davy, P., Lacoste, A., 2019. Landscape dynamics revealed by luminescence signals of feldspars from fluvial terraces. *Scientific Reports* 9, 8569

This article is protected by copyright. All rights reserved.

Brauderick, C. A., Dietrich, W. E., Leverich, G. T., and Sklar, L. S, 2009. Experimental evidence for the conditions necessary to sustain meandering in coarse-bedded rivers, *Proceedings of the National Academy of Sciences*, 106, 16936–16941

Brocard, G.Y., Willenbring, J.K., Miller T.E., Scatena, F.N., 2016. Relict landscape resistance to dissection by upstream migrating knickpoints. *Journal of Geophysical Research*: *Earth Surface* 121, 1182-1203.

Buffington, J.M., Montgomery, D.R., 1997. A systematic analysis of eight decades of incipient motion studies, with special reference to gravel-bedded rivers. *Water Resources Research* 33 (8), 1993-2029

Chatanantavet, P., Parker, G., 2008. Experimental study of bedrock channel alluviation under varied sediment supply and hydraulic conditions. *Water Resources Research* 44, W12446

Cook, K.L., Turowski, J.M., Hovius, N., 2013. A demonstration of the importance of bedload transport for fluvial bedrock erosion and knickpoint propagation. *Earth Surface Processes and Landforms* 38, 683-695.

Cook, K.L., Turowski, J.M., Hovius, N., 2014. River gorge eradication by downstream sweep erosion. *Nature Geoscience* 7, 682-686

Croissant, T., Lague, D., Steer, P., Davy, P., 2017. Rapid post-seismic landslide evacuation boosted by dynamic river width. *Nature Geoscience* 10, 680-684

Davy, P., Croissant, T., Lague, D., 2017. A precipiton method to calculate river hydrodynamics, with applications to flood prediction, landscape evolution

This article is protected by copyright. All rights reserved.

models, and braiding instabilities. *Journal of Geophysical Research: Earth Surface* 122, 1491–1512

DiBiase, R.A., Whipple, K.X., Lamb, M.P., Heimsath, A.M., 2015. The role of waterfalls and knickzones in controlling the style and pace of landscape adjustment in the western San Gabriel Mountains, California. *Geological Society of America Bulletin* 127(3–4), 560–583

Dijk, W., Lageweg, W., and Kleinhans, M, 2012. Experimental meandering river with chute cutoffs, *J. Geophys. Res.-Earth*, 117, doi:10.1029/2011JF002314

Dubinski, I.M., Wohl, E., 2013, Relationships between block quarrying, bed shear stress, and stream power: A physical model of block quarrying of a jointed bedrock channel. *Geomorphology* 180-181, 66-81.

Duvall, A., Kirby, E., Burbank, D., 2004. Tectonic and lithologic controls on bedrock channel profiles and processes in coastal California. *Journal of Geophysical Research* 109, F03002

Finnegan, N.J., Balco, G., 2015. Sediment supply, base level, braiding, and bedrock river terrace formation: Arroyo Seco, California, USA. *Geological Society of America Bulletin* 125 (7/8), 1114-1124

Finnegan, N.J., Roe, G., Montgomery, D.R., Hallet, B., 2005. Controls on the channel width of rivers: Implications for modelling fluvial incision of bedrock. *Geology* 33, 229-232.

Finnegan, N.J., Sklar, L.S., Fuller, T.K., 2007. Interplay of sediment supply, river incision, and channel morphology revealed by the transient evolution of an

This article is protected by copyright. All rights reserved.

experimental bedrock channel. *Journal of Geophysical Research* 112, F03S11

Finnegan, N.J., Klier, R.A., Johnstone, S., Pfeiffer, A.M., Johnson, K., 2017. Field evidence for the control of grain size and sediment supply on steady0state bedrock river channel slopes in a tectonically active setting. *Earth Surface Processes and Landforms* 42, 2338-2349

Gilbert, G.K., 1877. *Report on the Geology of the Henry Mountains*. US Government Printing Office, Washington D.C.

Glover, R E. and Florey, Q.L., 1951. *Stable channel profiles*, Tech. rep., U.S. Bur. Reclamation, Denver, CO, USA.

Golly A., Turowski, J.M., Badoux, A., Hovius, N., 2017. Controls and feedbacks in the coupling of mountain channels and hillslopes. *Geology* 45 (4), 307-310

Hartshorn, K., Hovius, N., Dade, W.B., Slingerland, R.L., 2002. Climate-Driven Bedrock Incision in an Active Mountain Belt. *Science* 297, 2036-2039

Heron, D.W. (custodian), 2014. *Geological map of New Zealand 1:250,000*. GNS Science geological map 1. GNS Science, Lower Hutt.

Hooke, R., 1968. Model geology: Prototype and laboratory streams: Discussion. *Geological Society of America Bulletin* 79, 391-394

Ikeda, S., Parker, G., and Kimura, Y., 1988. Stable width and depth of straight gravel rivers with heterogeneous bed materials, *Water Resources Research* 24, 713–722

This article is protected by copyright. All rights reserved.

Johnson, J.P.L., Whipple, K.X., 2007. Feedbacks between erosion and sediment transport in experimental bedrock channels. *Earth Surface Processes and Landforms* 32, 1048-1062

Johnson, J.P.L., Whipple, K.X., 2010. Evaluating the controls of shear stress, sediment supply, alluvial cover, and channel morphology on experimental bedrock incision rate. *Journal of Geophysical Research* 115, F02018

Johnson, J.P.L., Whipple, K.X., Sklar, L.S., Hanks, T.C., 2009. Transport slopes, sediment cover, and bedrock channel incision in the Henry Mountains, Utah. *Journal of Geophysical Research* 114, F02014

Lacey, G., 1930. Stable channels in alluvium, in: *Minutes of the Proceedings of the Institution of Civil Engineers*, Thomas Telford-ICE Virtual Library, 229, 259–292

Lague, D., 2010. Reduction of long-term bedrock incision efficiency by short-term alluvial cover intermittency. *Journal of Geophysical Research: Earth Surface* 115, F02011

Lague, D., 2014. The stream power incision model: evidence, theory and beyond. *Earth Surface Processes and Landforms* 39 (1) 38–61

Lague, D., Brodu, N., Leroux, J., 2013. Accurate 3D comparison of complex topography with terrestrial laser scanner: Application to the Rangitikei canyon (N-Z). *ISPRS Journal of Photogrammetry and Remote Sensing* 82, 10-26

Lajeunesse, E., Malverti, L., Charru. F., 2010. Bed load transport in turbulent flow at the grain scale: Experiments and modeling. *Journal of Geophysical Research* 115, F04001.

This article is protected by copyright. All rights reserved.

Lamb, M.P., Dietrich, W.E., 2009. The persistence of waterfalls in fractured rock. *Geological Society of America Bulletin* 121, 1123-1134

Lamb, M.P., Dietrich, W.E., Sklar, L.S., 2008. A model for fluvial bedrock incision by impacting suspended and bed load sediment. *Journal of Geophysical Research* 113, F03025.

Lavé, J., Avouac, J.P., 2001. Fluvial incision and tectonic uplift across the Himalayas of central Nepal. *Journal of Geophysical Research* 106 (B11), 26,561-26,591

Lee, J.M., Bland, K. Townsend, D.B. Kamp, P.J.J. (compilers), 2011. *Geology of the Hawke's Bay area: scale 1:250,000*. Institute of Geological & Nuclear Sciences 1:250,000 geological map 8. Institute of Geological & Nuclear Sciences Limited, Lower Hutt. 93 p. + 1 folded map

Li., T., Fuller, T.K., Sklar, L.S., Gran, K.B., Venditti, J.G., 2020. A mechanistic model for lateral erosion of bedrock channel banks by bedload particle impacts. *Journal of Geophysical Research Earth Surface* https://doi.org/10.1029/2019JF005509

Litchfield, N., Rieser, U., 2005. OSL age constraints for fluvial aggradation terraces and loess in the eastern North Island, New Zealand. *New Zealand Journal of Geology and* Geophysics 48, 581-589

Métivier, F. and Meunier, P, 2003. Input and Output mass flux correlations in an experimental braided stream. Implications on the dynamics of bed load transport, *J. Hydrol*., 271, 22–38

Métivier, F., Lajeunesse, E., Devauchelle, O., 2017. Laboratory rivers: Lacey's law, threshold theory, and channel stability. *Earth Surface Dynamics* 5, 187-198

This article is protected by copyright. All rights reserved.

Meyer-Peter, E., Muller, R., 1948. *Formulas for bed-load transport*, paper presented at the 2nd Meeting of International Association for Hydraulic Research. Stockholm.

Milne, J.D.G., 1973. *Maps and sections of river terraces in the Rangitikei Basin, North Island, New Zealand, N. Z*. Soil Surv. Rep. 4, Dep. of Sci. and Ind. Res., Wellington

Montgomery, D.R., Gran, K.B., 2001. Downstream variations in the width of bedrock channels. *Water Resources Research* 37 (6), 1841-1846

Nelson, P.A., Seminara, G., 2011. Modeling the evolution of bedrock channel shape with erosion from saltating bed load. *Geophysical Research Letters* 38, L17406

Paola, C., Straub, K.M., Mohrig, D.C., Reinhardt, L., 2009. The “unreasonable effectiveness” of stratigraphic and geomorphic experiments. *Earth-Science Reviews* 97, 1-43

Parker, G., Wilcock, P.R., Paola, C., Dietrich, W.E., Pitlick, J., 2007. Physical basis for quasi-universal relations describing bankfull hydraulic geometry of single-thread gravel bed rivers. *Journal of Geophysical Research* 112, F04005

Peakall, J., Ashworth, P. J., and Best, J. L., 2007. Meander-bend evolution, alluvial architecture, and the role of cohesion in sinuous river channels: a flume study, *J. Sediment. Res.*, 77, 197–212

Pfeiffer, A.M., Finnegan, N.J., Willenbring, J.K., 2017. Sediment supply controls equilibrium channel geometry in gravel rivers. *Proceedings of the National Academy of Sciences* 114 (13), 3346-3351

This article is protected by copyright. All rights reserved.

Phillips, C.B., Jerolmack, D.J., 2016. Self-organization of river channels as a critical filter on climate signals. *Science* 352, 694-697

Pillans, B., McGlone, M., Palmer, A., Mildenhall, D., Alloway, B., and Berger, G., 1993. The last Glacial maximum in central and southern North Island, New Zealand: a paleoenvironmental reconstruction using the Kawakawa Tephra Formation as a chronostratigraphic marker. *Palaeogeography, Palaeoclimatology, Palaeoecology* 101, 283-304.

Proust, J-N., Lamarche, G., Nodder, S., and Kamp, P.J.J., 2005. Sedimentary architecture of a Plio-Pleistocene pro- to back-arc basin, Wanganui Basin, New Zealand: *Sedimentary Geology* 181, 107-145.

Rees, C. Palmer, J., Palmer, A., 2017. Gilbert-style Pleistocene fan delta reveals tectonic development of North Island Axial ranges, New Zealand. *New Zealand Journal of Geology and Geophysics* 61, 64-78

Reitz, M. D., Jerolmack, D. J., Lajeunesse, E., Limare, A., Devauchelle, O., and Métivier, F., 2014. Diffusive evolution of experimental braided rivers, *Phys. Rev. E*, 89, 052809, doi:10.1103/PhysRevE.89.052809

Sapozhnikov, V. and Foufoula-Georgiou, E, 1996. Self-affinity in braided rivers, *Water Resour. Res*., 32, 1429–1439

Scheingross, J.S., Brun, F., Lo, D.Y., Omerdin, K., Lamb, M.P., 2014. Experimental evidence for fluvial bedrock incision by suspended and bedload sediment. *Geology* 42 (6), 523-526

Schumm, S.A., Mosley, M.P., and Weaver, W.E., 1987. Experimental Fluvial Geomorphology, John Wiley & Sons, Chichester, UK

This article is protected by copyright. All rights reserved.

Shobe, C.M., Tucker, G.E., Barnhart, K.R., 2017. The SPACE 1.0 model: a Landlab component for 2-D calculation of sediment transport, bedrock erosion, and landscape evolution. *Geoscientific Model Development* 10, 4577-4604

Sklar, L.S., Dietrich, W.E., 2001. Sediment and rock strength controls on river incision into bedrock. *Geology* 29, 1087-1090

Sklar, L.S., Dietrich, W.E., 2004. A mechanistic model for river incision into bedrock by saltating bed load. *Water Resources Research* 40, W06301.

Stark, C., 2006. A self-regulating model of bedrock river geometry. *Geophysical Research Letters* 33, L04402.

Stebbings, J., 1963. The shapes of self-formed model alluvial channels, in: *Minutes of the Proceedings of the Institution of Civil Engineers*, Thomas Telford-ICE Virtual Library, 25, 485–510

Tal, M. and Paola, C., 2007. Dynamic single-thread channels maintained by the interaction of flow and vegetation, Geology, 35, 347–350

Turowski, J.M., 2007, Controls on bedrock channel morphology: Experimental and theoretical investigations and comparison with natural channels [Ph.D. thesis]: Cambridge, UK, University of Cambridge, http://ethos.bl.uk/Order-Details.do?uin=uk.bl.ethos.613289.

Turowski, J.M., 2018. Alluvial cover controlling the width, slope and sinuosity of bedrock channels. *Earth Surface Dynamics* 6, 29-48.

Turowski, J.M., 2020. Mass balance, grade and adjustment timescales in bedrock channels. *Earth Surface Dynamics* 8, 103-122

This article is protected by copyright. All rights reserved.

Turowski, J.M., Hodge, R., 2017. A probabilistic framework for the cover effect in bedrock erosion. *Earth Surface Dynamics* 5, 311-330

Turowski, J.M., Lague, D., Hovius, N., and Crave, A., 2005, Dynamics and steadystate geometry of an experimental channel incising cohesive material: paper EGU05-A-05294 presented at the European Geosciences Union General Assembly, Vienna, Austria, 24–29 April 2005.

Turowski, J.M., Lague, D., Crave, A., Hovius, N., 2006. Experimental channel response to tectonic uplift. *Journal of Geophysical Research* 111, F03008.

Turowski, J.M., Lague, D., Hovius, N., 2007. Cover effect in bedrock abrasion: A new derivation and its implications for the modelling of bedrock channel morphology. *Journal of Geophysical Research* 111, F03008.

Turowski, J.M., Hovius, N., Meng-Long, H., Lague, D., Men-Chiang, C., 2008. Distribution of erosion across bedrock channels. *Earth Surface Processes and Landforms* 33 (3), 353-363

Turowski, J.M., Bockli, M., Rickenmann, D., Beer, A.R., 2013. Field measurements of the energy delivered to the channel bed by moving bed load and links to bedrock erosion. *J Geophys Res Earth Surf* 118, 2438-2450

Warburton, J., 1996. A brief review of hydraulic modelling of braided gravel bed rivers, *J. Hydrol. New Zealand*, 35, 157–174

Whipple, K.X., 2001. Fluvial landscape response time: how plausible is steady-state denudation? *American Journal of Science* 301, 313-325

Whipple, K.X., Tucker, G.E., 1999. Dynamics of the stream-power river incision model: Implications for height limits of mountain ranges, landscapes response

This article is protected by copyright. All rights reserved.

Accepted Article

timescales, and research needs. *Journal of Geophysical Research* 104 (B8), 17,661-17,674

Whitbread, K., Jansen, J., Bishop, P., Attal, M., 2015. Substrate, sediment and slope controls on bedrock channel geometry in postglacial streams. *Journal of Geophysical Research: Earth Surface* 120 (5), 779-798

Whittaker, A.C., Cowie, P.A., Attal, M., Tucker, G.E., Roberts G.P., 2007. Bedrock channel adjustment to tectonic forcing: Implications for predicting river incision rates. *Geology* 25 (2), 103-106.

Wohl, E.E., Anthony, D.J., Madsen, S.W., Thompson, D.M., 1996. A comparison of surface sampling methods for coarse fluvial sediments. *Water Resources Research* 32, 3219-3226

Yanites, B.J., 2018. The dynamics of channel slope, width, and sediment in actively eroding bedrock river systems. *Journal of Geophysical Research.* https://doi.org/10.1029/2017JF004405

Yanites, B.J., Tucker, G.E., 2010. Controls and limits on bedrock channel geometry. *Journal of Geophysical Research* 115, F04019.

Yanites, B.J., Tucker, G.E., Mueller, K.J., Chen, Y-G., Wilcox, T., Huang, S-Y., Shi, K-W., 2010. Incision and channel morphology across active structures along the Peikang River, central Taiwan: Implications for the importance of channel width. *Geological Society of America Bulletin* 122, 1192-1208

Yanites, B.J., Becker, J.K., Madritsch, H., Schnellmann, M., Ehlers, T.A., 2017. Lithologic Effects on Landscape Response to Base Level Changes: A

This article is protected by copyright. All rights reserved.

Modeling Study in the Context of the Eastern Jura Mountains, Switzerland. *Journal of Geophysical Research*: *Earth Surface* 122 (11), 2196-2222

Acknowledgements

We thank Maxime Bernard and Claire Astrié for assistance in the field, Jean-Jacques Kermarrec for his support and assistance with the experiments, Francois Métivier for the loan of the sediment feeder, Philippe Davy for providing the Floodos code, Horizons Regional Council for providing the rainfall data, and GNS Science for providing the geological map. We thank Sam Johnstone and an anonymous reviewer for their comments which helped to improve this paper. This research was funded by (i) the European Union's Horizon 2020 research and innovation programme through a Marie Sklodowska-Curie Actions Individual Fellowship (no. 703230, to E.B) and the European Research Council (grant agreement no. 803721, to P.S), (ii) a British Society for Geomorphology Early Career Researcher grant (to E.B), (iii) the George Mason Centre for the Natural Environment of the University of Auckland (to E.B), and (iv) the EROQUAKE project funded by the Agence Nationale de la Recherche No. ANR-14-CE33-005 (to P.S).

Conflict of Interest Statement

The authors declare no conflict of interest.

Data availability

All data is available on request from the corresponding author.

This article is protected by copyright. All rights reserved.

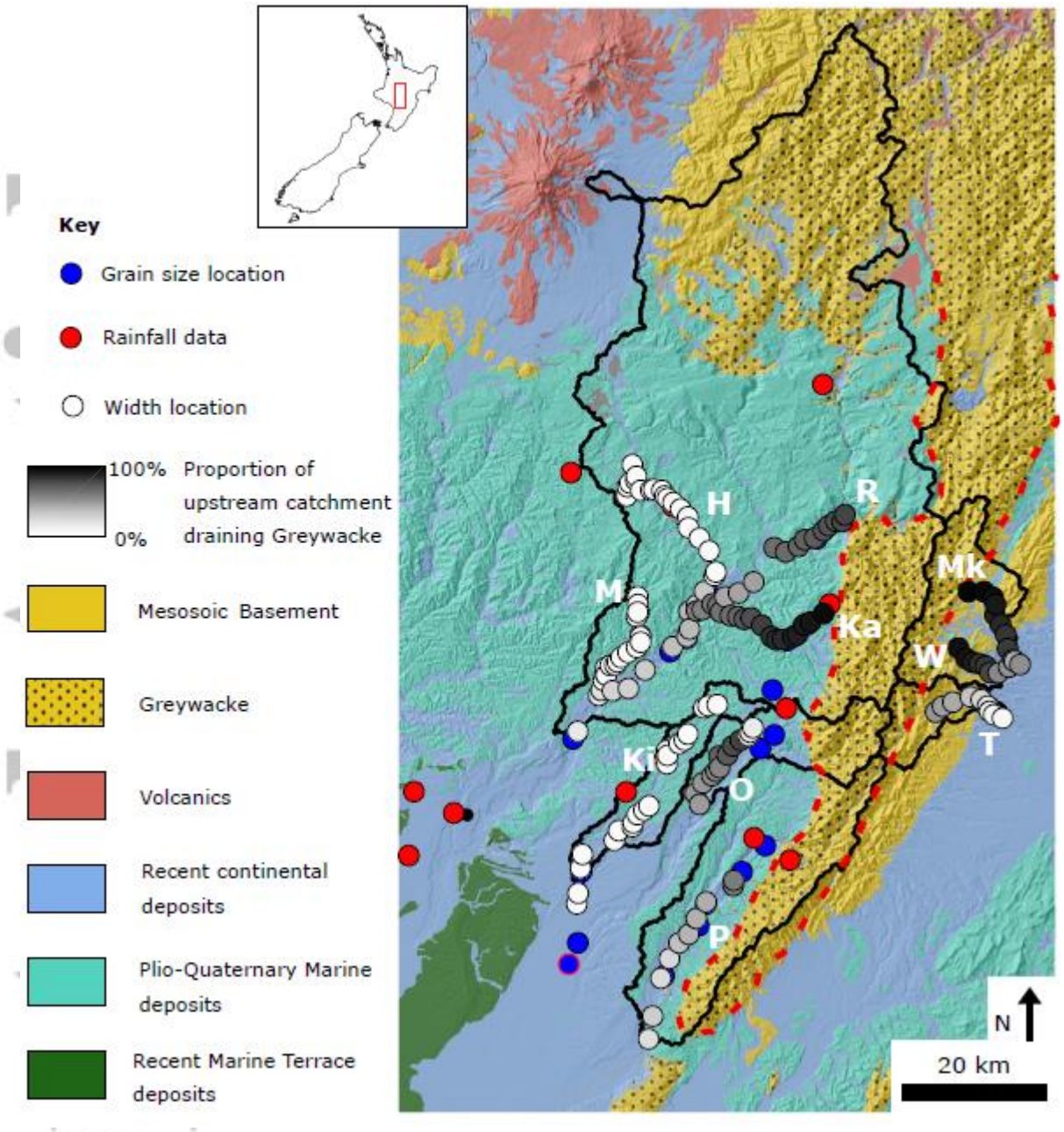


Figure 1

Study location, showing main outline of main catchments (black lines), width measurement locations (dots coloured from white to black by proportion of upstream drainage area draining greywacke), grain size measurement locations (blue dots), rainfall gauge stations (red dots) and the lithological map overlain onto a hillshade of the topography (from SRTM 90 m resolution data). White letters indicate the name of the rivers: R = Rangitikei, Ka = Kawhatau, H = Hautapu, M = Makohine, Ki = Kiwitea, O = Oroua, P = Pohangina, Mk = Makaroro, W = Waipawa, T =Tukituki. Modified from geological maps of Heron (2014) and Lee et al. (2011).

This article is protected by copyright. All rights reserved.

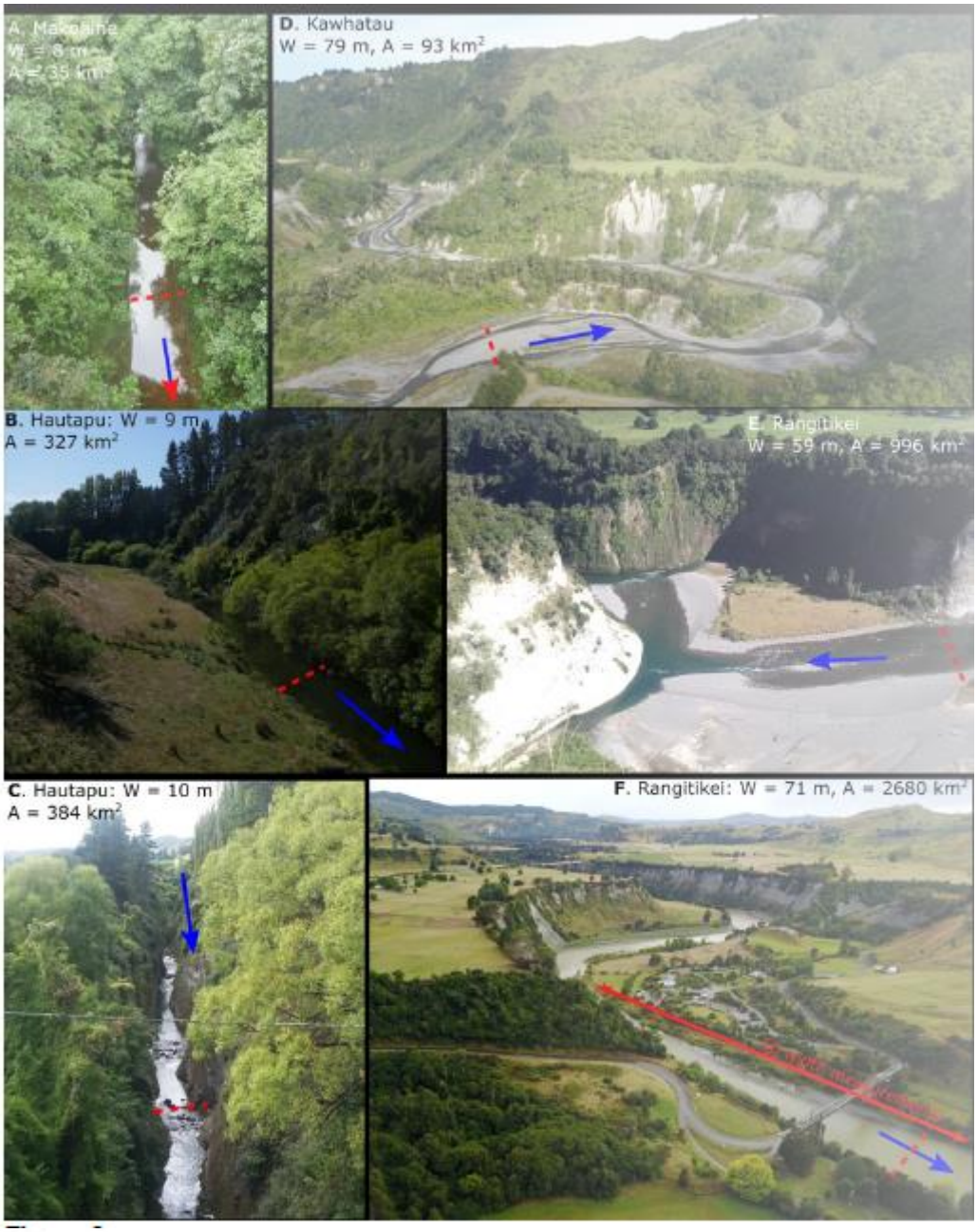


Figure 2

Photographs showing visual comparison of river morphology across the study area. A-C. Makohine and Hautapu rivers, draining solely sandstone and mudstone. D-F. Kawhatau and Rangitikei rivers, also eroding sandstone and mudstone at these locations but with an input of greywacke material from the Ruahine in the headwaters. Red dashed lines indicate how the channel width measurements were extracted. In F, repeat measurements of width were measured along a reach in order to determine the natural variability and uncertainty in the width measurements (see methods). Photo locations: (A) 39.78254° S, 175.73230° E, (B) 39.66897° S, 175.80450° E, (C) 39.71881° S, 175.84169° E, (D) 39.79151° S, 175.98599° E, (E) 39.68867° S, 176.00162° E, (F) 39.80980° S, 175.80855° E.

This article is protected by copyright. All rights reserved.

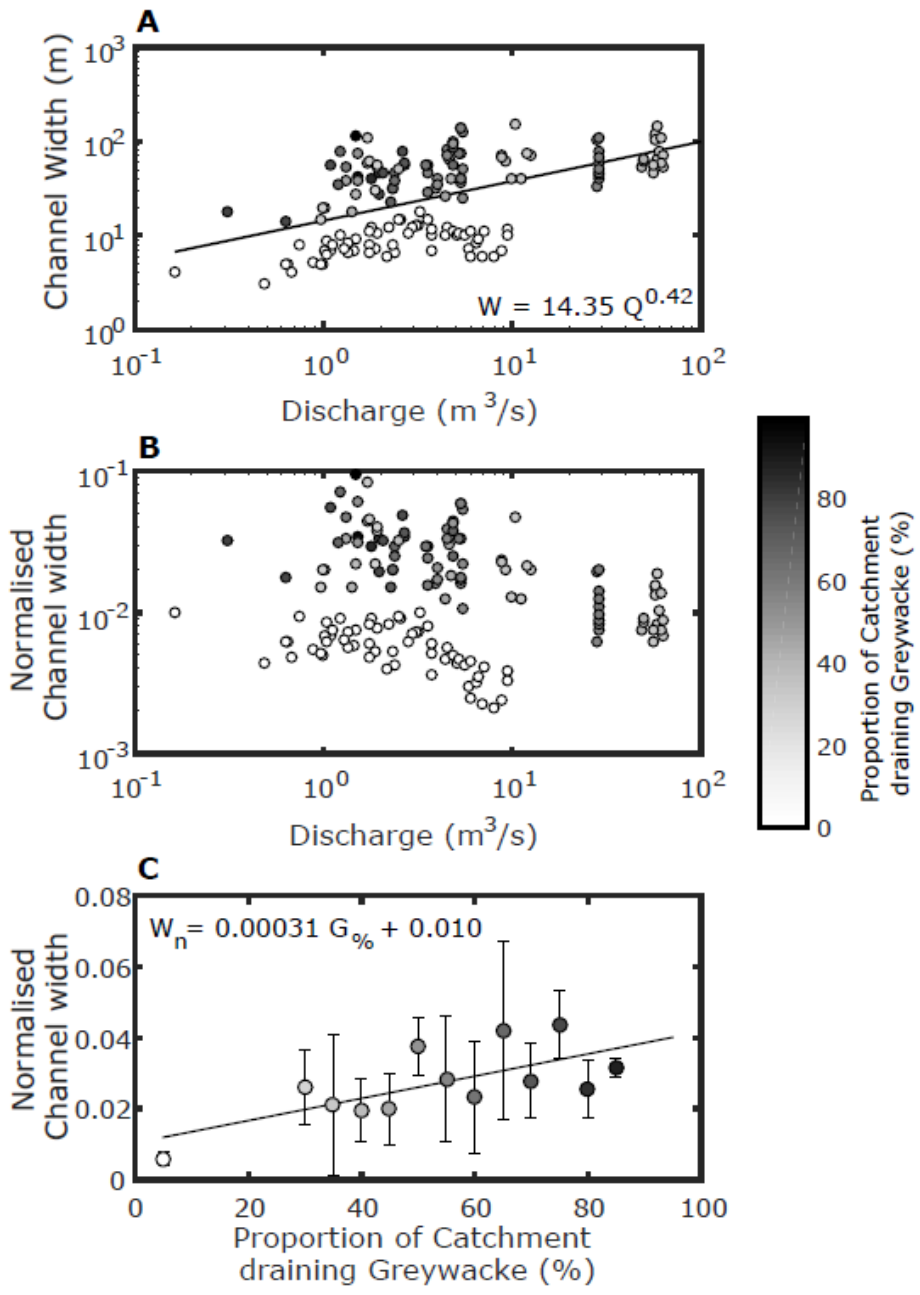


Figure 3

(A) Channel width against drainage area and discharge, for sites located within mudstone or sandstone, coloured by proportion of catchment draining greywacke. There is a clear distinction in the channel width between catchments that drain greywacke (grey/black) and those do not drain greywacke (open symbols). (B) Channel width normalised by the squareroot of discharge. For a given discharge, the channels that contain coarse sediment have a higher normalised channel width than those that do not contain sediment. (C) Relationship between normalised channel width and the proportion of the upstream drainage area that drains greywacke. Data plotted is the mean normalised channel width (with error bars ± 2 standard deviations) within bins of 5% range. R^2 = 0.481, p-value = 0.00859.

This article is protected by copyright. All rights reserved.

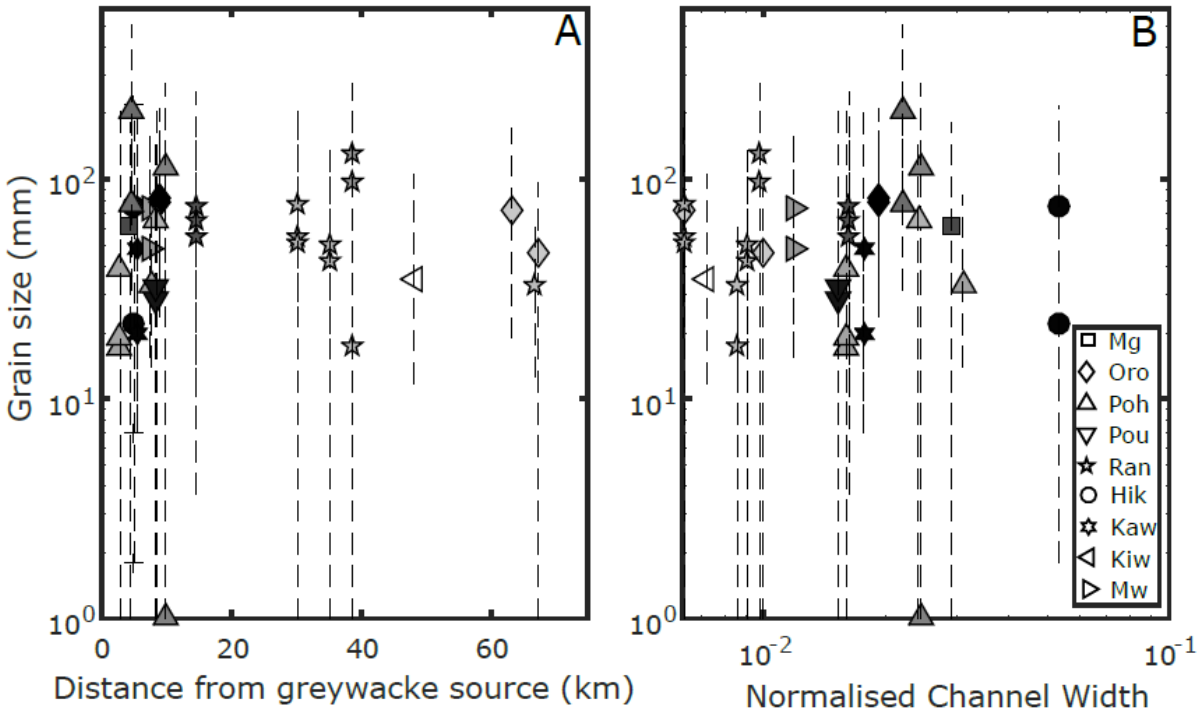


Figure 4

Sediment grain size data from across the study area, plotted against (A) the shortest transport distance from the front of the Ruahine mountain range, the source of the greywacke material and (B) normalised channel width. Points indicate the median grain size (D_{50}) while the dashed lines indicate the range between the D_{10} and D_{90} values of the grain size distribution. There is no clear effect of sediment grain size on the channel width across the study rivers. Labels: Mg = Mangoira. Oro = Oroua, Poh = Pohangina, Pou = Pourangaki, Ran = Rangitikei, Hik = Hikurangi, Kaw = Kawhatau, Kiw = Kiwitea, Mw = Mangawharariki.

Accepted Article

This article is protected by copyright. All rights reserved.

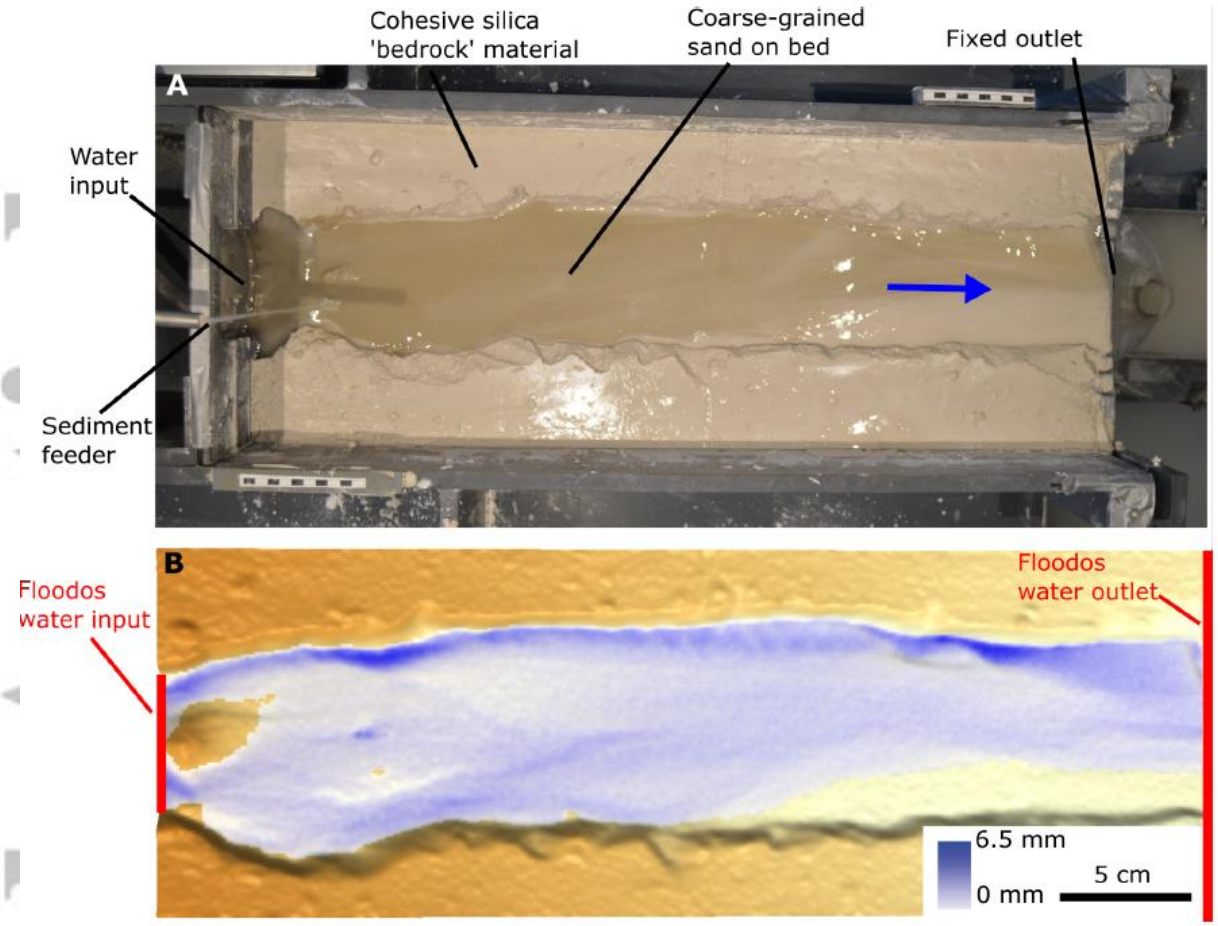


Figure 5

(A) Plan-view of experiment performed in the 80 cm x 30 cm Bedrock River Experimental Incision Tank at Université de Rennes. Flow direction is indicated by the blue arrow. (B) DEM generated from point cloud, with water depth mask generated by Floodos numerical hydrodynamic model (Davy et al., 2017) at same time step as (A). Red lines indicate the input and outlet for the water flow in Floodos, and the modelled grid matches the extent of the DEM.

Accepted

This article is protected by copyright. All rights reserved.

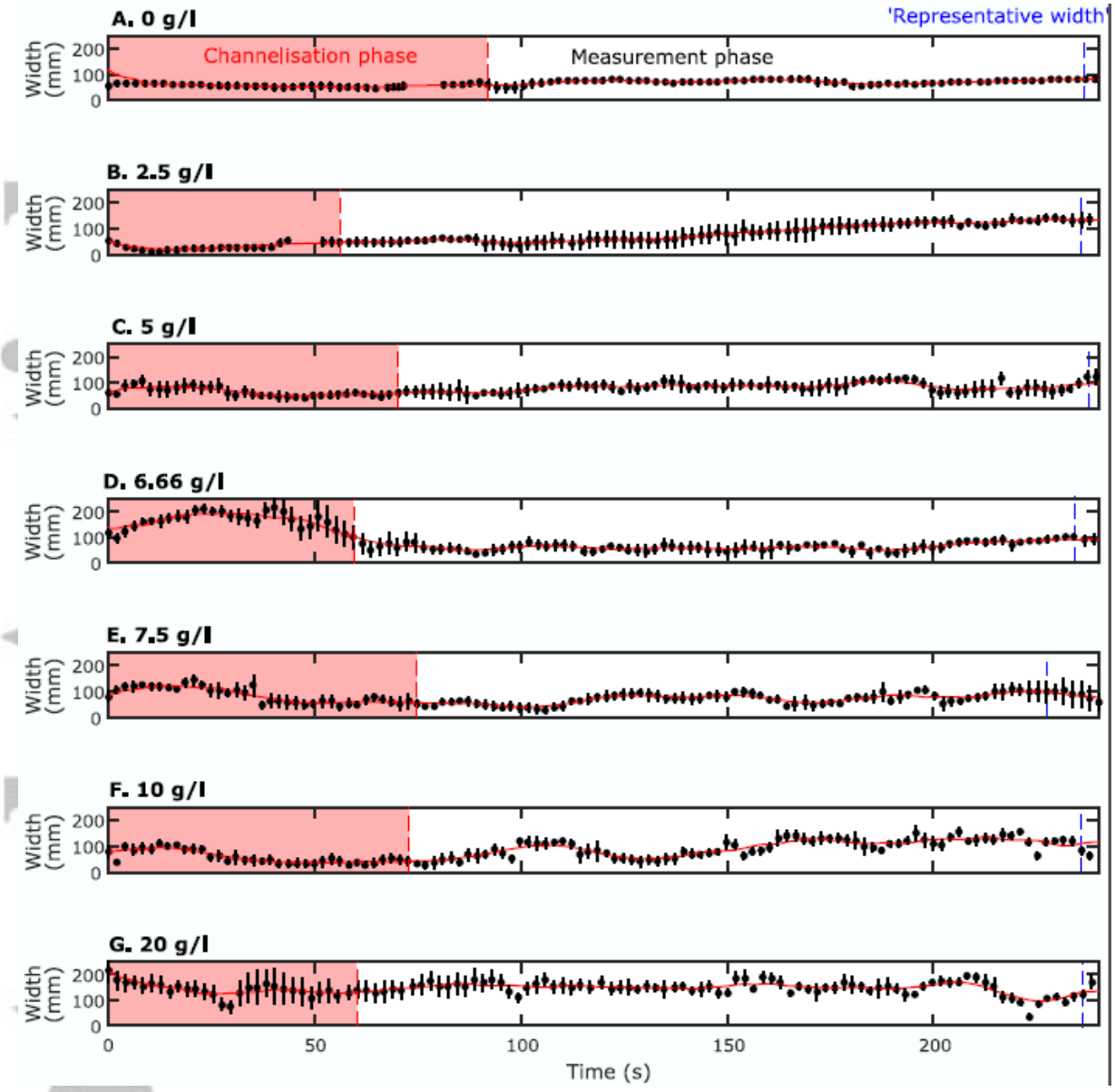


Figure 6

Evolution of mean channel width (except upper and lower 20 cm of channel) for all channel cross-sections during each of the seven sediment supplies (A-G). Data from the upper and lower 20 cm of the channel was not used to avoid any impact of boundary conditions on the channel width. Errorbars indicate ± 2 standard deviations from the mean value. Solid red line is a 10 point moving average through the data. The shaded red box and red dashed line indicates the period at the start of the experiment when a channel is initiated, i.e., when the initial incision due to the knickpoint had fully propagated through the channel. Measurements of channel geometry in subsequent figures were made after this initial phase. Blue dashed line indicates the timing of the DEMs extracted for 'representative' measurements. Labels indicate the sediment flux during each corresponding time period.

This article is protected by copyright. All rights reserved.

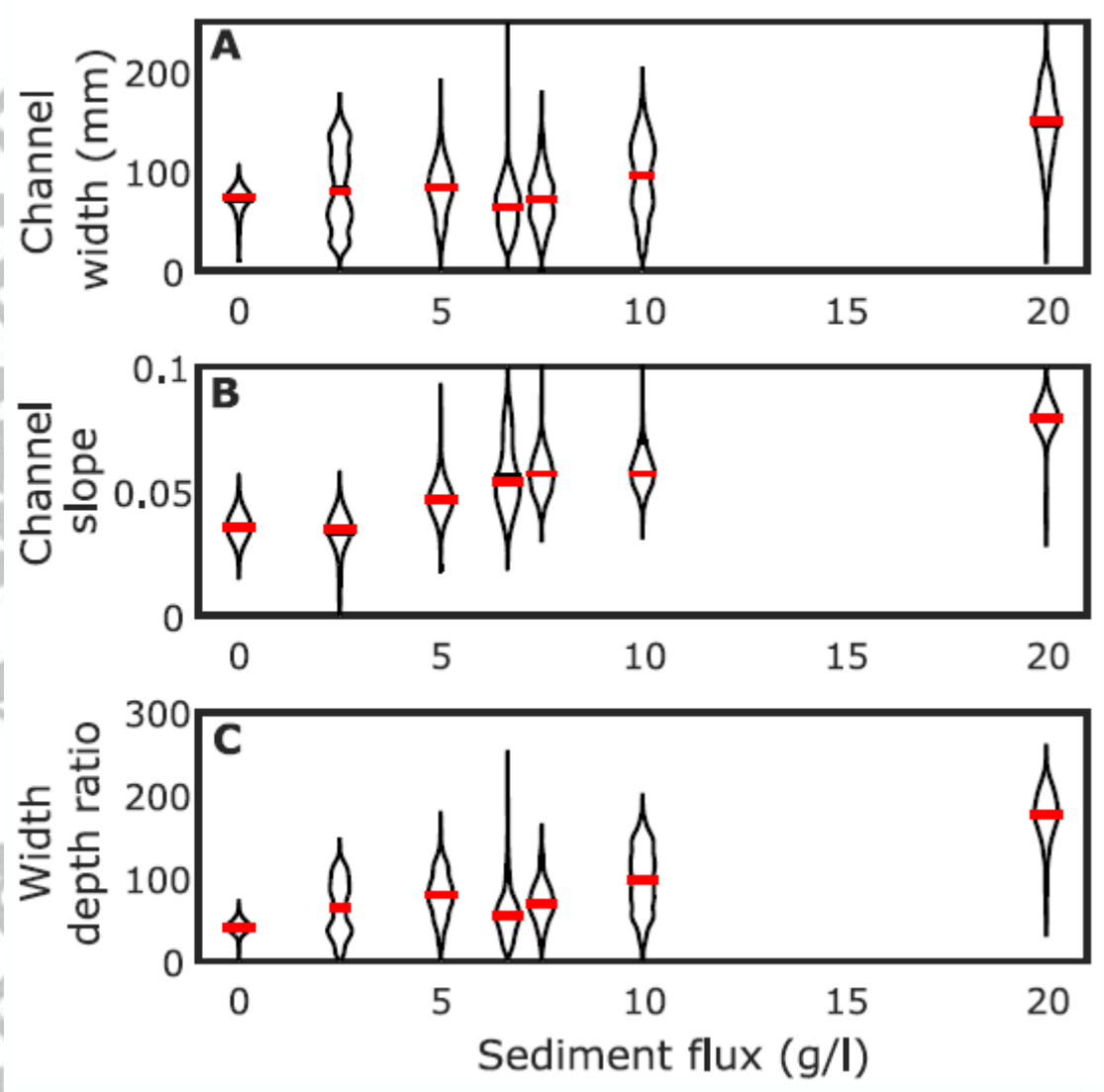


Figure 7

Violin plots showing the summary statistics for channel geometry under the different sediment supply conditions ranging from 0 to 20 g/l: (A) width, (B) slope, (C) width-depth ratio) . Plotted data was extracted from all cross-sections (except upper and lower 20 cm to avoid boundary effects) from all DEMs after the initial channel initialisation phase (see Fig. 6). Horizontal red bars indicate the median value, and horizontal black bars indicate the mean value. For reference, the width of the flume is 30 cm.

This article is protected by copyright. All rights reserved.

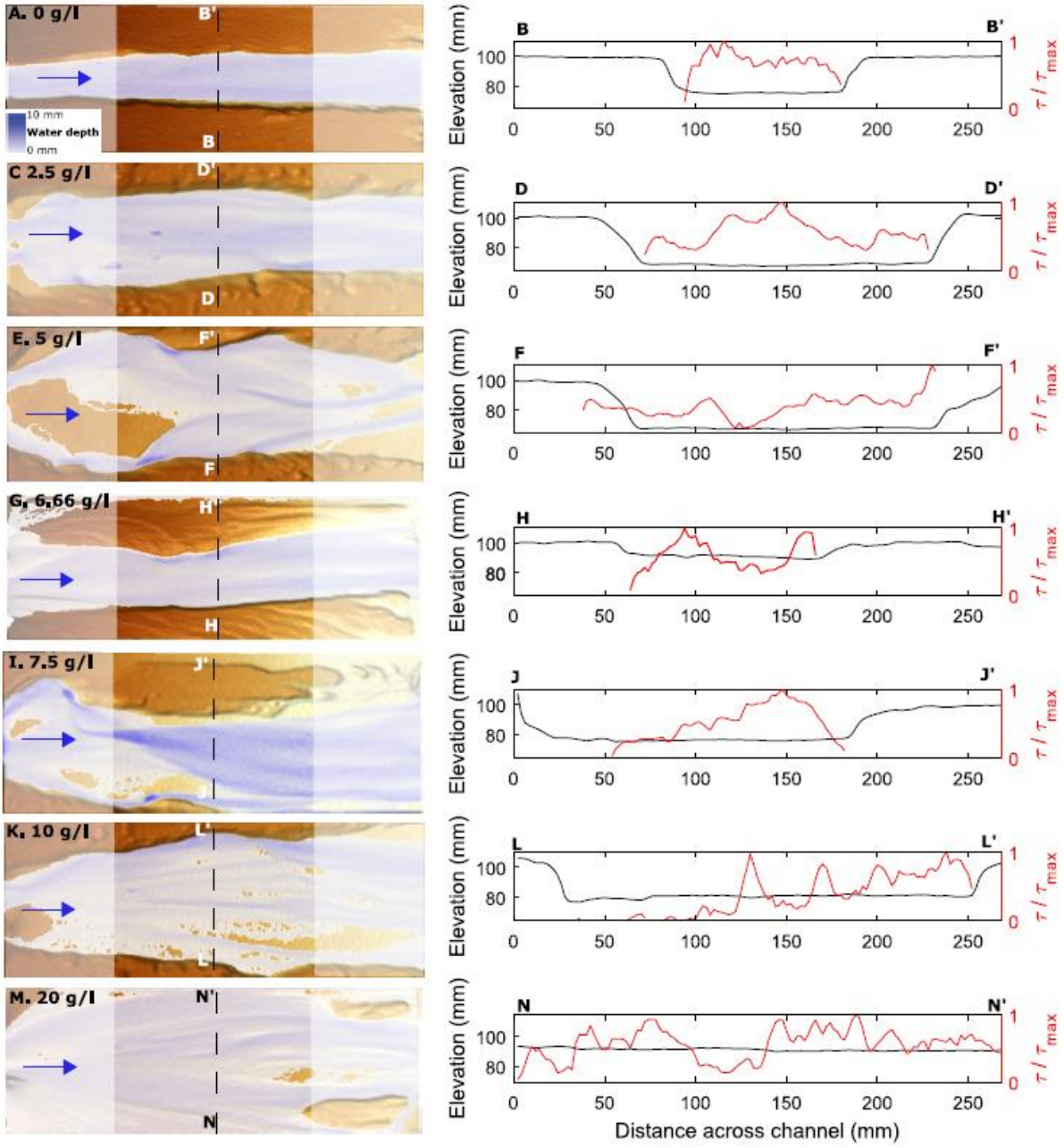


Figure 8

Left panel: Example representative DEMs (with water depth mask from Floodos model output) for the channels at each of the sediment fluxes (see also the photos in Fig. S8). White boxes at inlet and outlet highlight the limits of the analysis area, to avoid boundary effects of both the channel inlet and the channel outlet. Black dashed line shows the location of the channel cross-section extracted in the plots on the right panel, located at the channel mid-point. Red lines on the second y-axis on the cross-sections indicate the values of normalised shear stress (τ / τ_{max}).

This article is protected by copyright. All rights reserved.

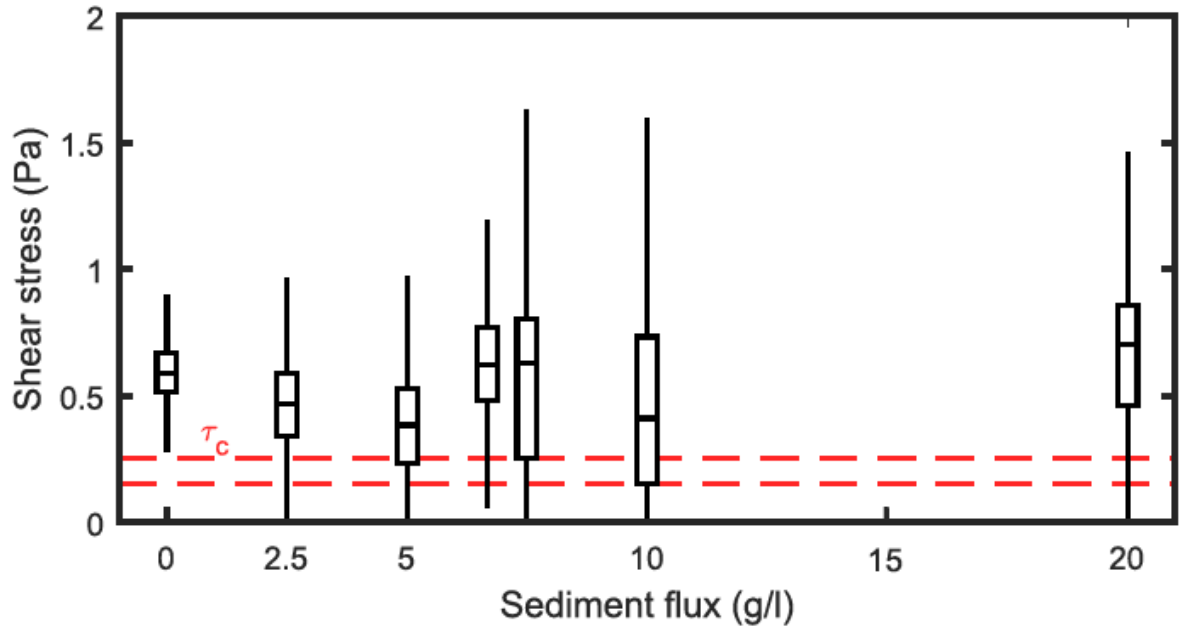


Figure 9

Box and whisker plot showing the distribution of shear stress within the channel under different sediment fluxes, from the 'representative' configurations. Dashed lines show the range of τ_c values (0.15 – 0.25 Pa) for the experimental channel. Horizontal black lines in the centre of the boxes indicate the median values, the edge of the boxes indicate the 25th and 75th percentiles.

Accepted

This article is protected by copyright. All rights reserved.

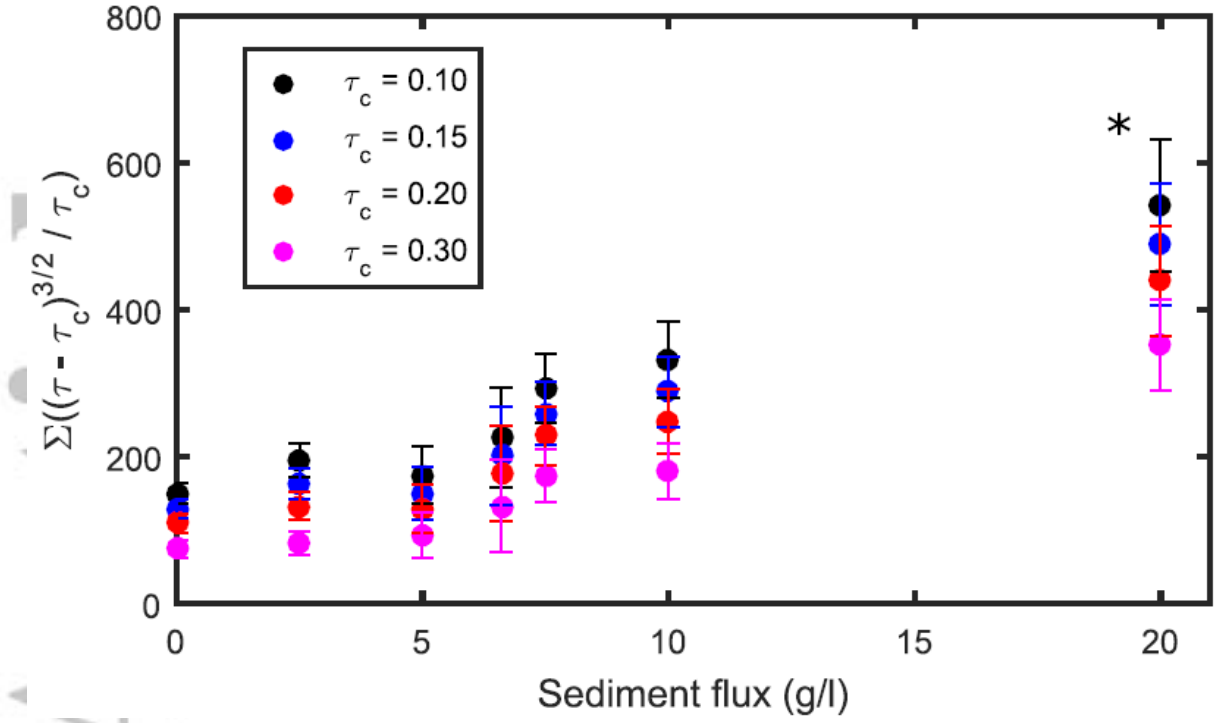


Figure 10

Mean total excess bedload shear stress (τ_{bl}) from 20 cross-sections across 10 DEMs leading up to the 'representative' conditions (total measurements = 200), to capture the spatial and temporal variability within the experiments. Different colours represent a sensitivity analysis of the impact of using different values for the critical shear stress. The star indicates some caution is required when interpreting the value when Q_s = 20 g/l, as the channel is sometimes constrained by the edges of the flume (Fig. 8M) and the channel has transitioned into an alluvial regime. Error bars indicate two standard deviations from the mean.

Accepted Article

This article is protected by copyright. All rights reserved.

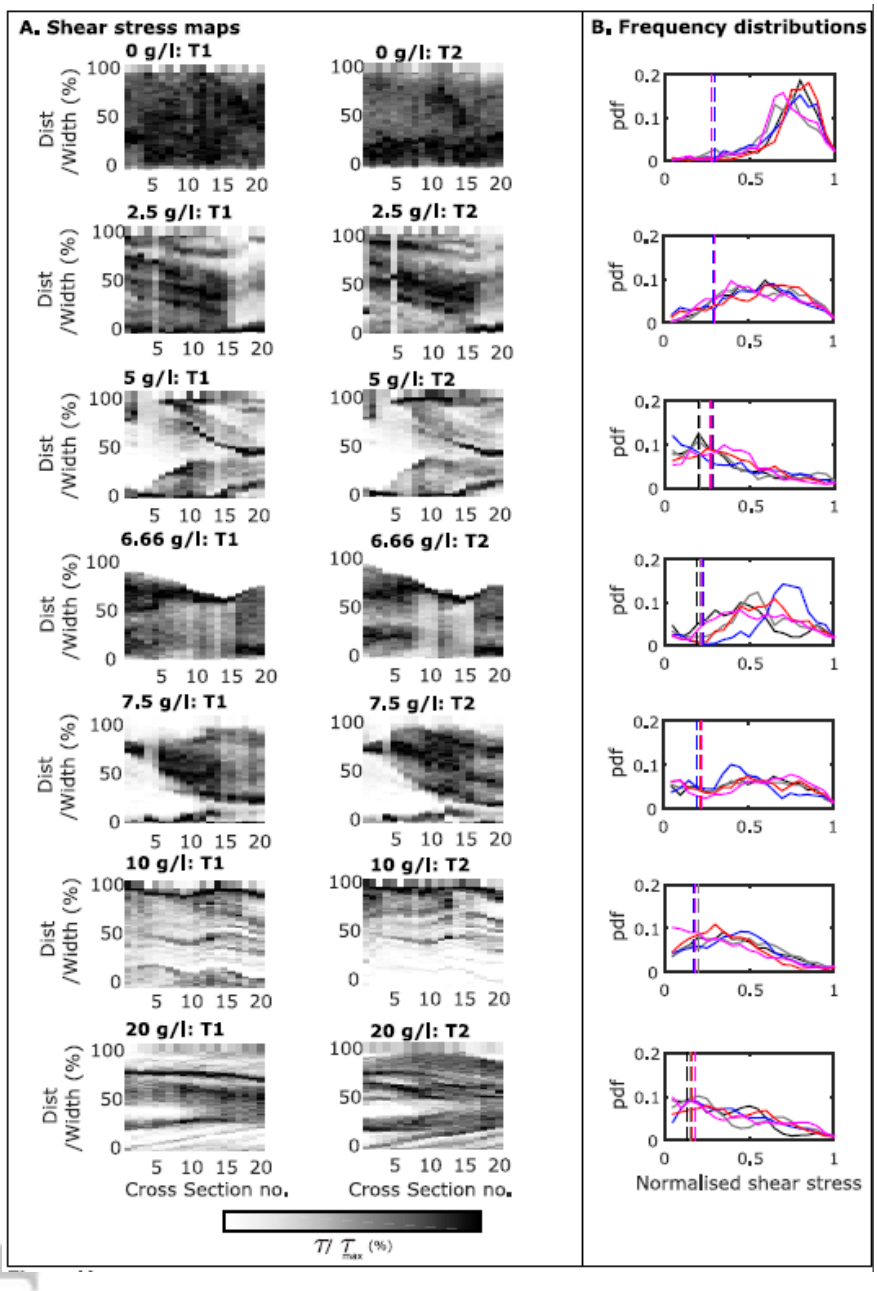


Figure 11

Visualisation of the distribution of normalised shear stress within the channel. For each sediment flux, twenty cross-sections were extracted from each of five DEMs which were collected at two-minute intervals. Normalised shear stress is calculated as the value of shear stress relative to the peak shear stress along each cross-section. The DEMs represent the five closest to 'representative' conditions. (A) the twenty cross-sections (normalised by width) for two of the DEMs (Time 1 and Time 2) for each of the sediment fluxes. Only two of the DEMs are plotted to save space, with the data from all five DEMs plotted in the probability density functions in (B). Where the majority of the points are coloured black, with little variability along a cross-section (e.g., when Q_s = 0 g/l), the distribution of shear stress is relatively uniform. Where there is a large variability in the colours across a cross section (e.g., Q_s = 20 g/l), the distribution is not uniform within the channel and multiple narrower channels are active across the channel bed which can be mostly inactive. In the

This article is protected by copyright. All rights reserved.

case of Q_s = 20 g/l, the location of these active channels is dynamic, with the pattern of distributed pattern of shear stress changing between the DEMs despite only being separated by two-minute intervals (shown by the reference arrows in red). (B) Probability density function (pdf) for each of the five DEMs (all twenty cross-sections included in the pdf) for values of normalised shear stress. The probability density functions were calculated through the frequency of the data points in bins. Dashed vertical lines indicate the critical shear stress normalised by the maximum shear stress. Consistency in the shape of the pdfs suggests that the nature of the shear stress distribution shown in the T1 and T2 DEMs is representative of the distribution of shear stress for a given sediment flux.

Accepted Article

This article is protected by copyright. All rights reserved.

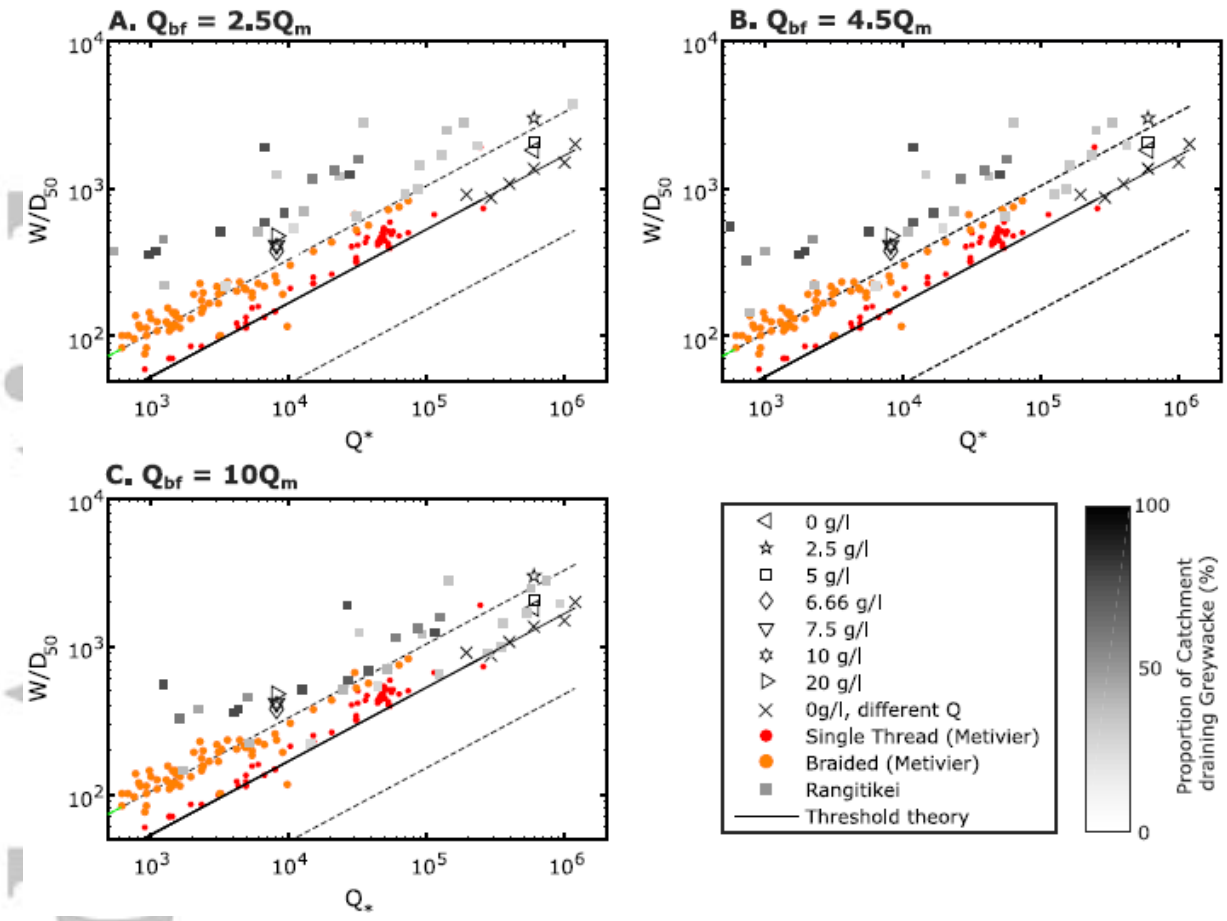


Figure 12

Comparison of data from this study against compilation of previous experiments including Baynes et al., 2018a (black crosses) and a comprehensive dataset of braided and single thread channels compiled in Métivier et al., 2017 (data in compilation from Stebbings, 1963; Schumm et al., 1987; Ikeda et al., 1988; Warburton, 1996; Sapozhnikov and Foufoula-Georgiou, 1996; Métivier and Meunier, 2003; Tal and Paola, 2007; Peakall et al., 2007; Brauderick et al., 2009; Dijk et al., 2012, Ashmore, 2013; Reitz et al., 2014). Black solid line is the threshold theory calculated when θ_t = 0.05, C_f = 0.1, as used by Métivier et al. (2017). Grey dashed lines indicate the uncertainty in the calculation of the threshold width due to uncertainty in the values used for the critical shear stress and friction coefficient. Upper grey dashed line calculated using θ_t = 0.03, C_f = 0.3, and lower grey dashed line calculated using θ_t = 0.3, C_f = 0.02. Panels A-C indicate a sensitivity analysis based on different values of the scaling factor to calculate the bankfull discharge (Q_{bf}) from the mean daily discharge (Q_m).

This article is protected by copyright. All rights reserved.

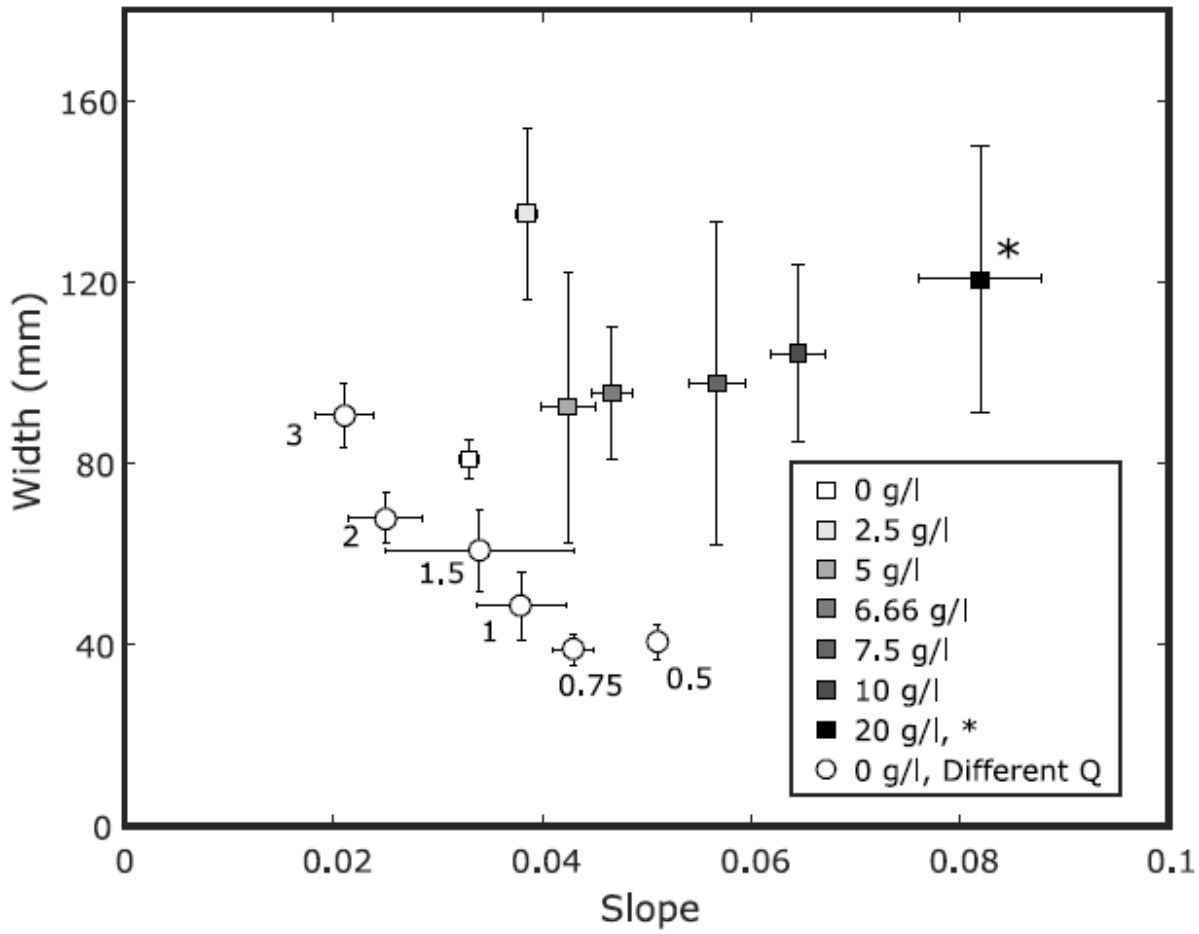


Figure 13

*Mean channel width against channel slope closest to 'representative width' for (i) the experiments in this study (squares), where sediment flux is variable but all points with a constant discharge of 1.5 l/min) and (ii) a reference dataset where Q_s = 0 g/l under different discharges between 0.5 – 3 l/min (white circles). Labels indicate the value of Q for each of these points (data from Baynes et al., 2018a). The channel width for the 20 g/l experiment was potentially limited by the width of the experimental box due to the unconstrained banks and dynamic migrating channel, and the true width may be larger than plotted, indicated by a *. The channel at 2.5 g/l remained constrained within banks of silica material and thus was not limited by the experimental box. Mean values of width and slope are from the five DEMs leading up to the representative conditions, with the error bars indicating two standard deviations from the mean.*

This article is protected by copyright. All rights reserved.

Table 1: Relationship between channel width and mean daily discharge for the individual tributaries. Power law relationship calculated using the 'logfit' function in Matlab.

River	Greywacke in headwaters?	Scaling between width and discharge
Rangitikei	Y	$W = 16.13Q^{0.38}$
Kawhatau	Y	$W = 33.65Q^{0.42}$
Pohangina	Y	$W = 90.27Q^{-0.12}$
Oroua	Y	$W = 18.68Q^{0.56}$
Makaroro	Y	$W = 136.43Q^{-1.64}$
Waipawa	Y	$W = 37.77Q^{0.67}$
Tuki	Y	$W = 17.87Q^{1.78}$
Hautapu	N	$W = 15.43Q^{-0.28}$
Makohine	N	$W = 6.55Q^{0.54}$
Kiwitea	N	$W = 6.65Q^{0.52}$
All catchments	-	$W = 14.35Q^{0.42}$

Accepted Article

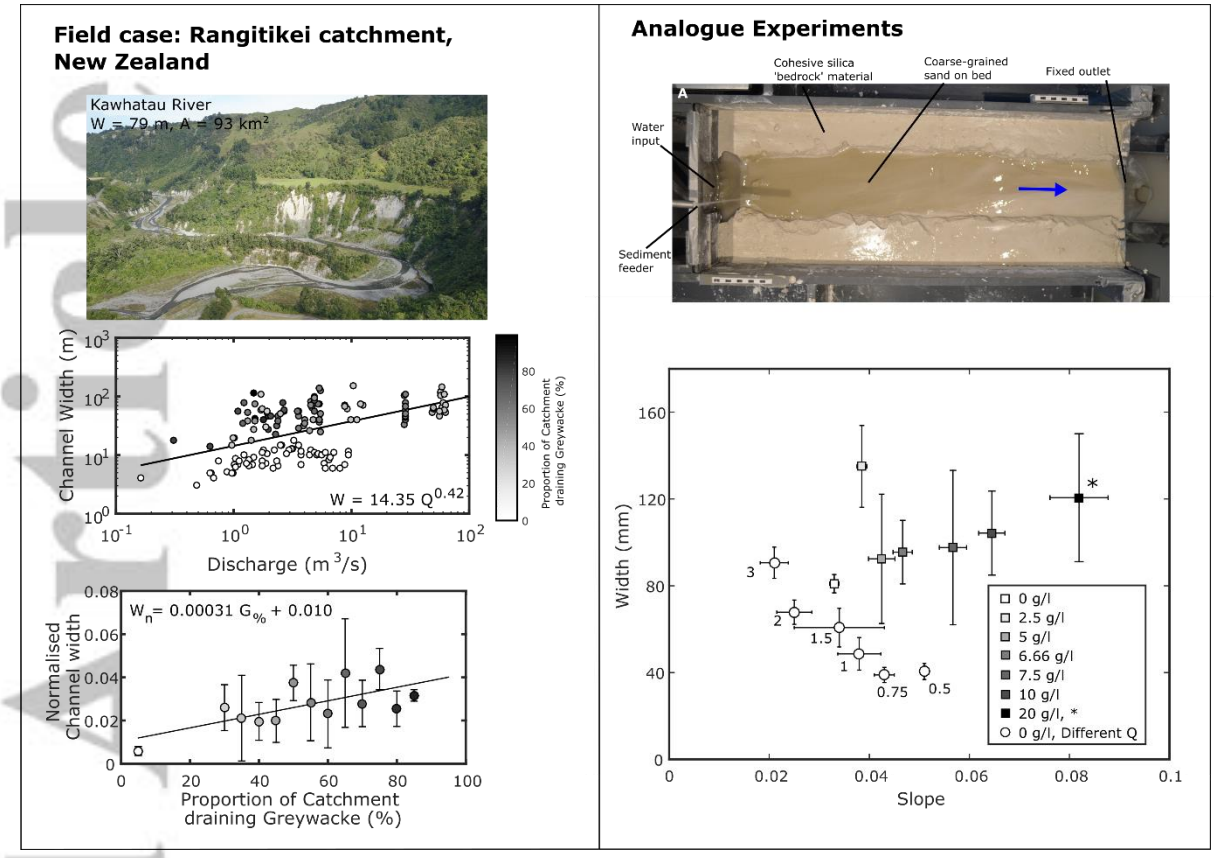
This article is protected by copyright. All rights reserved.

Accepted Article

Table 2: Parameters for the four experiments presented in this study

Experiment number	Discharge (l /min)	Sediment flux (g/l)
1	1.5	0
2	1.5	2.5
3	1.5	5
4	1.5	6.66
5	1.5	7.5
6	1.5	10
7	1.5	20

This article is protected by copyright. All rights reserved.



Accepted Article

This article is protected by copyright. All rights reserved.